Article

Green Synthesis and Bioactivity of Aliphatic N-Substituted Glycine Derivatives

Ameneh Jafari, Mahboube Eslami Moghadam,* and Hassan Mansouri-Torshizi
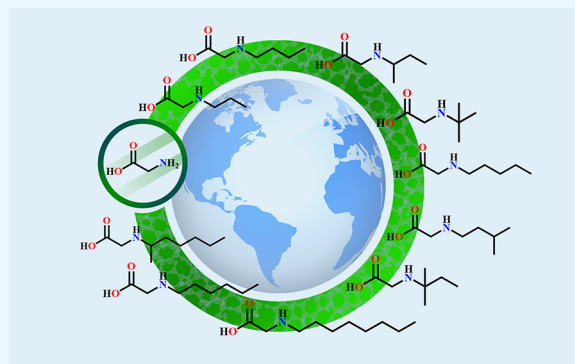
Read Online

ACCESS | Metrics & More | Article Recommendations | Supporting Information

ABSTRACT: Standard amino acids have an asymmetric α-carbon atom to which $-$COOH, $-$NH$_2$, $-$H, and $-$R groups are bonded. Among them, glycine is the simplest (R = $-$H) with no asymmetric carbon, and other natural amino acids are C-substituted of glycine. Here, we have designed and made a green synthesis of some new N-substituted glycine derivatives with R$-$(NH)CH$_2$$-$COOH formula, where R is flexible and hydrophobic with different chain lengths and benches of the type propyl, butyl, *sec*-butyl, *tert*-butyl, pentyl, isopentyl, *tert*-pentyl, hexyl, 2-aminoheptyl, and octyl. These glycine derivatives were characterized by recording their melting points and FT-IR, mass, ^{1}H NMR, and ^{13}C NMR spectra. DFT studies revealed that 2-aminoheptyl glycine had the highest electronegativity value and can thus act as a good bidentate ligand for the metal centers. ADME comparative results and bioavailability radars indicated that both octyl- and 2-aminoheptyl glycine had the most lipophilicity, making them good agents in cell passing. Furthermore, lipophilicity determination showed that octyl glycine was the best and propylgly was more soluble than others. Based on solubility, lipophilicity, and dipole moment values, propyl- and 2-aminoheptyl-glycine were considered for bio-macromolecular interaction studies. Thus, the interaction of these two agents with DNA and HSA was studied using absorption spectroscopy and circular dichroism techniques. Due to the presence of the R-amine group, they can interact with the DNA by H-binding and hydrophobicity, while electrostatic mode could not be ruled out. Meanwhile, molecular docking studies revealed that octyl- and 2-aminoheptyl glycine had the highest negative docking energy, which reflects their higher tendency to interact with DNA. The DNA binding affinity of two candidate AAs was determined by viscosity measurement and fluorescence emission recording, which confirms that groove binding occurs. Also, the toxicity of these synthesized amino acid derivates was tested against the human foreskin fibroblast (HFF) cell line. They showed IC$_{50}$ values within the range of 127$-$344 μM after 48 h with the highest toxicity for 2-aminoheptyl glycine.

1. INTRODUCTION

Amino acids are the most abundant organic components in living cells for the formation, nitrogen balance, expansion, reproduction, and well-being of organisms of both humans and animals.[1] Glycine, with the chemical formula NH$_2$CH$_2$COOH, is an α-amino acid (AA) that exists in the form of a zwitterion as $^+$NH$_3$CH$_2$COO$^-$.[2] This simplest AA has the lowest molecular weight with protein forming. Also, it is the only amino acid that does not have an asymmetrical carbon atom, causing it to be nonoptical and without any L or D configuration.[3,4] As a side chain, the hydrogen atom of glycine allows it to conform to hydrophobic and hydrophilic situations within the polypeptide chain.[5] Glycine, as an essential AA, has multifunctional acts for metabolites; hence, the severe deficiency of glycine has undesirable effects on cytoprotection, health, low growth, decline of an immune response, and anomalous nutrient metabolism. This AA affects the cell membrane, the neurotransmitter in the central nervous system, quality of sleep, absorption, and digestion of vitamins and lipids, detoxification in the human body, creation of super-

oxide, conjugation of bile acids, *etc*. The major constituent of extracellular proteins such as elastin and collagen is glycine. Also, it has a crucial role in the prevention of many diseases and disorders such as cancer, obesity, and diabetes.[4,6]

Since the influence of glycine in life has been recognized and this substance has biological capability and can be used as a precursor in the synthesis of drugs in the future, the number of published studies in this scope has increased.[7] Because of basic amino and carboxylic acid groups, glycine is amphoteric.[8] So, it acts as a bidentate ligand and forms a closed ring structure with the metal ions, allowing a ligand to bind to the metal center more tightly. This condition would occur when the pH values
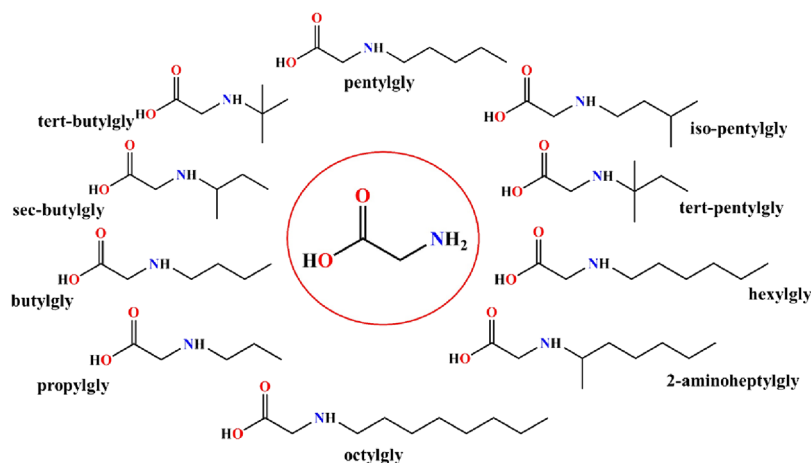
Scheme 1. Structures of Synthesized Glycine Derivatives

are more than 7. In addition, this ligand can act as a monodentate and coordinate with the metal ions *via* its carboxylate group under low pH values.[9,10]

In recent years, the study of "how transition metal complexes bind to DNA" has been crucial for the advancement of DNA molecule probes and chemotherapeutics. Numerous complexes have been synthesized and developed to identify anticarcinogens capable of recognizing and cleaving DNA, in which among them, amino acids have been considered as a ligand in drug-DNA binding and their significance in drug design.[11] A variety of compounds can bind to DNA and engage in interactions with it, resulting in alterations to both the structure of DNA and its base sequence. These changes ultimately lead to disruptions in the replication of DNA. Chemotherapeutic drugs interact with DNA through either covalent or noncovalent mechanisms.[12,13] It has been recognized that the design of new compounds with multimode binding capabilities can offer several advantages, such as improved administration methods and reduced toxicity. Additionally, these anticancer complexes, with different lipophilicities, contain a variety of metals or ligands that can be easily manipulated to suit specific applications.[14,15] The lipophilicity of any ligand will increase with the growing bulkiness aliphatic of R groups. The lipophilic group can enable drugs to penetrate the plasma membrane to bind to the goal DNA. Also, the hydrophilic group can reduce the toxicity of drugs, and greater lipophilicity can enhance it by simplifying the passive uptake of drug molecules across the lipidic cell membrane.[16]

Over the last decades, the assessment of solvent type has become a crucial aspect of the global pharmaceutical industry's development. Eight of the most widely used solvents were identified as potentially dangerous due to their toxicity or fire and explosion risks: dichloromethane, 1,2-dichloroethane, chloroform, 1,4-dioxane, diethyl ether, diisopropyl ether, *n*-hexane, and 1,2-dimethoxyethane.[17,18] In this regard, the synthesis of glycine derivatives has been carried out by nongreen solvents and tough situations over the past years. For example, the synthesis of butylgly, 2-aminoheptylgly, and propylgly has been done at 60−110 °C by hydrothermal or reflux methods.[5,19−21] Nevertheless, the most important defect in the synthesis of some compounds such as pentylgly, hexylgly, octylgly, *etc.*, is the use of hazardous solvents such as dichloromethane, benzene, toluene, *etc.*[22−25]

As glycine and its derivatives are very decisive ligands in bioinorganic chemistry, this article explains a safe way to synthesize N-substituted glycine derivatives bearing three to eight aliphatic carbon chains, where R is propyl, butyl, *sec*-butyl, pentyl, isopentyl, *tert*-pentyl, hexyl, 2-aminoheptyl, and octyl without utilizing a toxic solvent *via* green chemistry (see Scheme 1 where all the reactions have been done in water). In the following, various experimental techniques such as FT-IR, UV−vis, mass, ^{1}H NMR, and ^{13}C NMR spectrometries were used for the characterization of these compounds. Pharmacokinetics, physicochemical activities, and medicine-likeness were calculated using the SwissADME free-online web tool. The lipophilicity of these AA derivatives has been determined *via* the shake-flask procedure. Also, density functional theory was evaluated for obtaining the quantum chemical parameters and validating the structures. Additionally, the interaction and binding parameters of DNA and HSA with these amino acids have been studied through docking calculations as well as by experimental approaches including UV−vis, fluorescence, and circular dichroism spectroscopies and viscosity measurement. Finally, the toxicity of all synthesized compounds was tested against the Human foreskin fibroblasts (HFF) cell line. These glycine derivatives may act as bidentate ligands and can be used (i) to carry bioactive metal ions into biological systems or (ii) to make their metal complexes as well as to investigate their uses as serious agents in drug design, bactericide or fungicide pesticides, insecticides, antitumor agents, *etc.*
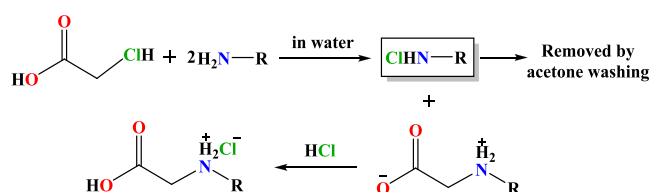
2. EXPERIMENTAL SECTION

2.1. Materials and Instrumentation. Propylamine, butylamine, *sec*-butylamine (α-chiral amine), *tert*-butylamine, pentylamine, isopentylamine, *tert*-pentylamine, hexylamine, 2-aminoheptylamine (α-chiral amine), octylamine, chloroacetic acid, glycine, and hydrochloric acid were purchased from Sigma-Aldrich and Merck. Acetone and *n*-octanol were of analytical grade and used as received. IR spectra were collected on an FT-IR 8400 Shimadzu spectrometer using KBr pellets. The mass spectra were scanned using a model CH7A Varian (EI, 70 eV) mass spectrometer. ^{1}H NMR (300 MHz) and ^{13}C NMR (75 MHz) spectra were recorded on a Bruker BRX-250 Avance spectrometer. Chemical shifts for ^{1}H were referenced to the residual proton in the DMSO-*d₆* solvent. Melting points were measured using a BUCHI melting point B-545 apparatus. Further, through a SPEKOL 2000 UV 6800 recording

spectrophotometer, the absorbance was measured. A Jasco J-1500 CD spectrometer was employed to measure the circular dichroism. A Jasco J-1500 CD spectrometer and a Hitachi MPF-4 spectrofluorimeter were employed to measure the circular dichroism and the fluorescence emissions, respectively. Viscosity measurement was studied by an Ostwald micro-viscometer (Schott-Geräte). The optical density (OD) was measured spectrophotometrically at 570 nm via a BioTek-ELx800 Eliza microplate reader.

2.2. Green Synthesis of R-Glycine. A solution of alkyl amine (22 mmol) in 3 mL of cold water was added dropwise to 3 mL of aqua-solution of chloroacetic acid (0.945 g, 10 mmol) in an ice bath and was stirred constantly for 24 h. Then, water was removed by a rotary evaporator completely until a white precipitate was observed. Prepared chloride salt was washed with acetone extra pure several times, and the final product was obtained by acidifying with HCl to pH = 2 and slow evaporation at RT and recrystallized with HCl (1 M) (see Scheme 2).

Scheme 2. Preparation Route of Glycine Derivatives[a]

[a]R: propyl, butyl, *sec*-butyl, *tert*-butyl, pentyl, isopentyl, *tert*-pentyl, hexyl, 2-aminoheptyl, octyl.

2.2.1. Glycine (as Reference). NH$_2$CH$_2$COOH; C$_2$H$_5$NO$_2$: 75.03 g/mol; ^{1}H NMR (300 MHz, DMSO-d_6, δ in ppm): 2.94 (s, 2H, CH$_2$), 7.29 related to NH$_2$ (br, 2H); ^{13}C NMR (75 MHz, DMSO-d_6, δ in ppm): 41.1 (s, 1C$_{CH2}$), 170.2 (s, 1C=O).

2.2.2. Propylgly·HCl. (CH$_3$(CH$_2$)$_2$NHCH$_2$COOH)·HCl; C$_5$H$_{12}$ClNO$_2$: 153.61 g/mol; Yield: 47%; m.p. 197.5 °C; IR (cm^{-1}, solid): 3559−3673 (w, O−H), 3102 (w, N-H), 2962 (m, C-H), 1747 (s, C=O), 1417 (s, C−O), 1214 (m, C−N); ^{1}H NMR (300 MHz, DMSO-d_6, δ in ppm): 0.86 (t,$^3J_{H-H}$ = 6 Hz, 3H, CH$_3$), 1.62 (m, 2H, CH$_2$), 2.81 (t,$^3J_{H-H}$ = 6 Hz, 2H, CH$_2$), 3.73 (s, 2H, CH$_2$), and 9.32 related to NH amine (br, H); ^{13}C NMR (75 MHz, DMSO-d_6, δ in ppm): 10.9 (s, 1C), 18.7 (s, 1C), 47.0 (s, 1C), 48.2 (s, 1C), 167.9 (s, 1C=O); MS (70 eV, EI): m/z (%): 116 (48) [M]$^+$, 72 (92) [M−COOH]$^+$, 60 (81) [M-C$_4$H$_9$N]$^+$, 30 (100) [CH$_3$N]$^+$.

2.2.3. Butylgly·HCl. (CH$_3$(CH$_2$)$_3$NHCH$_2$COOH)·HCl; C$_6$H$_{14}$ClNO$_2$: 167.63 g/mol; Yield: 53%; m.p. 198.2−200.0 °C; IR (cm^{-1}, solid): 3300−3500 (w, O−H), 3193 (w, N−H), 2941 (s, br, C−H), 1752 (s, C=O), 1417 (s, C−O), 1216 (m, C−N); ^{1}H NMR (300 MHz, DMSO-d_6, δ in ppm): 0.87 (t,$^3J_{H-H}$ = 6 Hz, 3H, CH$_3$), 1.30 (m, 2H, CH$_2$), 1.61 (m, 2H, CH$_2$), 2.87 (m, 2H, CH$_2$), 3.81 (s, 2H, CH$_2$), and 9.27 related to NH amine (br, H); ^{13}C NMR (75 MHz, DMSO-d_6, δ in ppm): 13.4 (s, 1C), 19.2 (s, 1C), 27.2 (s, 1C), 46.4 (s, 1C), 46.7 (s, 1C), 168.0 (s, 1C=O); MS (70 eV, EI): m/z (%): 131 (76) [M], 87 (88) [M−COOH]$^+$, 60 (78) [M-C$_5$H$_{11}$N]$^+$, 28 (100) [C=O].

2.2.4. sec-Butylgly·HCl. (CH$_3$CH$_2$CHCH$_3$NHCH$_2$COOH)·HCl; C$_6$H$_{14}$ClNO$_2$: 167.63 g/mol; Yield: 57%; m.p. 207.6 °C; IR (cm^{-1}, solid): 3343−3504 (w, O−H), 3275 (w, N−H), 2965 (s, br, C−H), 1752 (s, C=O), 1419 (s, C−O); 1224 (m, C−N); ^{1}H NMR (300 MHz, DMSO-d_6, δ in ppm): 0.89 (t,$^3J_{H-H}$ = 6 Hz, 3H, CH$_3$), 1.20 (d,$^3J_{H-H}$ = 3 Hz, 3H, CH$_3$), 1.46 (m, H, CH$_2$), 1.79 (m, H, CH$_2$), 3.09 (s, H, CH), 3.90 (m, 2H, CH$_2$), and 8.96 related to NH amine (br, H); ^{13}C NMR (75 MHz, DMSO-d_6, δ in ppm): 14.9 (s, 1C), 20.0 (s, 1C), 30.2 (s, 1C), 49.5 (s, 1C), 59.5 (s, 1C); MS (70 eV, EI): m/z (%): 130 (13) [M]$^+$, 86 (73) [M−COOH]$^+$, 56 (100) [C$_4$H$_6$]$^+$, 30 (97) [CH$_3$N]$^+$.

2.2.5. tert-Butylgly·HCl. ((CH$_3$)$_3$CHNHCH$_2$COOH)·HCl; C$_6$H$_{14}$ClNO$_2$: 167.63 g/mol; Yield: 63%; m.p. 133 °C; IR (cm^{-1}, KBr disk): 3183 (w, N−H), 3060 (s, br, C−H), 1758 (s, C=O), 1359 (s, C−O); 1216 (m, C−N); ^{1}H NMR (300 MHz, DMSO-d_6, δ in ppm): 1.28 (s, 9H, 3CH$_3$), 3.75 (t,$^3J_{H-H}$ = 6 Hz, 2H, CH$_2$), and 9.19 related to NH amine (br, H); ^{13}C NMR (75 MHz, DMSO-d_6, δ in ppm): 24.9 (s, 3C), 41.6 (s, 1C), 56.2 (s, 1C), 168.3 (s, 1C=O); MS (70 eV, EI): m/z (%): 130 (2) [M]$^+$, 85 (23) [M$^+$−COOH]$^+$, 70 (100) [C$_4$H$_8$]$^+$, 30 (100) [CH$_3$N]$^+$.

2.2.6. Pentylgly·HCl. (CH$_3$(CH$_2$)$_4$NHCH$_2$COOH)·HCl; C$_7$H$_{16}$ClNO$_2$: 181.66 g/mol; Yield: 53%; m.p. 130−135 °C; IR (cm^{-1}, solid): 3482−3648 (w, O−H), 2948 (s, br, C−H), 1752 (s, C=O), 1421 (s, C−O), 1218 (m, C−N); ^{1}H NMR (300 MHz, DMSO-d_6, δ in ppm): 0.85 (m, 3H, CH$_3$), 1.26 (m, 4H, 2CH$_2$), 1.61 (m, 2H, CH$_2$), 2.85 (s, 2H, CH$_2$), 3.81 (m, 2H, CH$_2$), 9.22 (br, H, NH), and 13.68 (br, H, OH); ^{13}C NMR, δ, ppm: 13.7 (s, 1C), 21.6 (s, 1C), 24.8 (s, 1C), 28.0 (s, 1C), 46.7 (s, 1C), 46.8 (s, 1C), 168.0 (s, 1C=O); MS (70 eV, EI): m/z (%): 145 (74) [M], 101 (83) [M−COOH], 44 (87) [COOH]$^+$, 28 (100) [C=O].

2.2.7. Isopentygly·HCl. ((CH$_3$)$_2$CH-(CH$_2$)$_2$NHCH$_2$COOH)·HCl; C$_7$H$_{16}$ClNO$_2$: 181.66 g/mol; Yield: 61%; m.p. 198−201 °C; IR (cm^{-1}, solid): 3473−3741 (w, O−H), 2950 (s, br, C−H), 1749 (s, C=O), 1423 (s, C−O), 1222 (m, C−N); ^{1}H NMR (300 MHz, DMSO-d_6, δ in ppm): 0.85 (d,$^3J_{H-H}$ = 6 Hz, 6H, 2CH$_3$), 1.55 (m, 3H, CH$_2$CH), 2.88 (m, 2H, CH$_2$), 3.80 (s, 2H, CH$_2$), 9.29 (br, H, NH), and 13.70 (br, H, OH); ^{13}C NMR, δ, ppm: 22.1 (s, 2C), 25.3 (s, 1C), 33.9 (s, 1C), 45.3 (s, 1C), 46.8 (s, 1C), 168.0 (s, 1C=O); MS (70 eV, EI): m/z (%): 145 (15) [M], 100 (34) [M−COOH]$^+$, 88 (93) [C$_3$H$_6$NO$_2$]$^+$, 42 (100) [C$_3$H$_6$]$^+$.

2.2.8. tert-Pentylgly·HCl. (CH$_3$CH$_2$CH-(CH$_3$)$_2$NHCH$_2$COOH)·HCl; C$_7$H$_{16}$ClNO$_2$: 181.66 g/mol; Yield: 43%; m.p. 203 °C; IR (cm^{-1}, solid): 3426−3648 (w, O−H), 3180 (w, N−H), 3052 (s, br, C−H), 1760 (s, C=O), 1355 (s, C−O), 1209 (m, C−N); ^{1}H NMR (300 MHz, DMSO-d_6, δ in ppm): 0.86 (t,$^3J_{H-H}$ = 9 Hz, 3H, CH$_3$), 1.22 (m, 6H, CH$_3$), 1.55 (q,$^3J_{H-H}$ = 6 Hz, 2H, CH$_2$), 3.89 (s, 2H, CH$_2$) and 8.07 related to NH amine (br, H); ^{13}C NMR, δ, ppm: 12.2 (s, 1C), 24.9 (s, 2C), 31.3 (s, 1C), 56.2 (s, 1C), 68.8 (s, 1C), 176.8 (s, 1C=O).

2.2.9. Hexylgly·HCl. (CH$_3$(CH$_2$)$_5$NHCH$_2$COOH)·HCl; C$_8$H$_{18}$ClNO$_2$: 195.69 g/mol; Yield: 72%; m.p. 225.4 °C; IR (cm^{-1}, solid): 3475−3648 (w, O−H), 3002 (w, N−H), 2931 (s, br, C−H), 1751 (s, C=O), 1419 (s, C−O), 1216 (m, C−N); ^{1}H NMR (300 MHz, DMSO-d_6, δ in ppm): 0.85 (t,$^eJ_{H-H}$ = 7.5 Hz, 2H, CH$_2$), 3.83 (s, 2H, CH$_2$), 9.05 (br, H, NH), and 13.71 (br, H, OH); ^{13}C NMR, δ, ppm: 13.8 (s, 1C), 21.8 (s, 1C), 25.1 (s, 1C), 25.6 (s, 2C), 30.7 (s, 1C), 46.8 (s, 1C), 168.0 (s, 1C=O); MS (70 eV, EI): m/z (%): 159 (10) [M], 114 (100) [M−COOH]$^+$, 100 (69) [C$_6$H$_{13}$N], 29 (92) [CHO]$^+$.

2.2.10. *2-Aminoheptylglgly·HCl.* (CH$_3$(CH$_2$)$_4$CHCH$_3$NHCH$_2$COOH)·HCl; C$_9$H$_{20}$ClNO$_2$: 209.71 g/mol; Yield: 57%; m.p. 218 °C; IR (cm^{-1}, KBr disk): 3440−3671 (w, O−H), 3142 (w, N−H), 2952 (s, br, C−H), 1749 (s, C=O), 1413 (s, C−O), 1170 (m, C−N); ^{1}H NMR (300 MHz, DMSO-d_6, δ in ppm): 0.88 (t,$^3J_{H-H}$ = 3 Hz, 3H, CH$_3$), 1.30 (m, 10H, CH$_3$, 7CH$_2$), 1.46 (m, H, CH$_2$), 1.76 (m, H, CH$_2$), 3.84 (s, 2H, CH$_2$), 9.16 (br, H, NH), and 13.75 (br, H, OH); ^{13}C NMR (75 MHz, DMSO-d_6, δ in ppm): 14.3 (s, 1C), 15.7 (s, 1C), 22.3 (s, 1C), 24.9 (s, 1C), 31.3 (s, 1C), 32.2 (s, 1C), 44.6 (s, 1C), 53.8 (s, 1C), 168.7 (s, 1C=O); MS (70 eV, EI): m/z (%): 173 (2) [M], 157 (65) [M−OH], 102 (100) [M−C$_5$H$_{11}$]$^+$, 29 (93) [CHO]$^+$.

2.2.11. *Octylglgly·HCl.* (CH$_3$(CH$_2$)$_7$NHCH$_2$COOH)·HCl; C$_{10}$H$_{22}$ClNO$_2$: 222.74 g/mol; Yeild: 67%; m.p. 232 °C; IR (cm^{-1}, solid):): 3480−3650 (w, O−H), 2931(s, br, C−H), 1751 (s, C=O), 1423 (s, C−O), 1220 (m, C−N); ^{1}H NMR (300 MHz, DMSO-d_6, δ in ppm): 0.85 (t,$^3J_{H-H}$ = 7.5 Hz, 3H, CH$_3$), 1.26 (m, 10H, 5CH$_2$), 1.61 (m, 2H, CH$_2$), 2.85 (t,$^3J_{H-H}$ = 7.5 Hz, 2H, CH$_2$), 3.80 (s, 2H, CH$_2$), 9.25 (br, H, N−H); ^{13}C NMR, δ, ppm: 13.9 (s, 1C), 22.0 (s, 1C), 25.1 (s, 1C), 25.9 (s, 1C), 28.4 (s, 2C), 31.1 (s, 1C), 46.6 (s, 1C), 46.7 (s, 1C), 168.0 (s, 1C=O); MS (70 eV, EI): m/z (%): 186 (20) [M]$^+$, 144 (92) [C$_7$H$_{14}$NO$_2$]$^+$, 88 (100) [C$_3$H$_5$NO$_2$]$^+$, 29 (93) [CHO]$^+$.

The mass, ^{1}H NMRand , ^{13}C NMR spectra and numbering data of all AAs are given in Figures S1−S20 and Tables S1−S11 in the Supporting Information, respectively.

2.3. DFT Calculations. All quantum mechanical simulation studies of AAs have been completed by density functional theory (DFT) with the hybrid function B3LYP. All calculations were performed using the latest version of the Gaussian09 program and were then generated using the program Gauss view 6.0.16. The 6-31g(d) basis set in the water phase was used for the C, H, N, and O atoms. The frequency calculations (Opt-Freq) were applied at their minimum energy to compare the experimental and theoretical infrared spectra. Next, all compounds' molecular electrostatic potential (MEP) surfaces were investigated to obtain their most positive and negative regions in the interactions with possible biomacromolecules.[26,27]

2.4. Solubility and Lipophilicity. The lipophilicity value of the AA derivatives was measured *via* the "shake flask" procedure utilizing *n*-octanol of analytical grade/doubly distilled water phase partition.[28,29] As stated in the OECD guidelines, there are some compounds for which there is no advanced technique to calculate their concentration in the solution (for example there is no proper absorption peak in their UV−vis spectra), and thus their solubility cannot be determined.[30,31] In these cases, a proper amount of each synthesized compound should be added to *n*-octanol and distilled water separately and shaken continuously for 24 h at room temperature to saturate these two phases. Next, the undissolved compounds were either centrifuged or filtered from saturated solutions and evaporated to complete dryness. The weight of the residue represents the solubility (S) of each synthesized compound.

Log$S$ and log$P$[28,29] were then computed using eqs 1 and 2.

$$\log S = \log[\text{ligand}]_{\text{in water}} \tag{1}$$

$$\log P = \log \frac{[\text{ligand}]_{\text{in octanol}}}{[\text{ligand}]_{\text{in water}}} \tag{2}$$

2.5. Bioactivity Prediction. *2.5.1. ADME Study.* SMILES files were created for each compound *via* chembio3D Ultra 14.0 after which the ADME (including the properties of absorption, distribution, metabolism, and excretion) profile of AA derivatives was predicted using the SwissADME tools. SwissADME is a free web tool (http://www.swissadme.ch) used to investigate the effect of the medicinal chemistry of molecules, pharmacokinetics, and drug-likeness on bioactive targets. Computer simulations, such as BOILED-Egg, iLOGP, and bioavailability radar have been done, and Lipinski's rule of five was investigated for all compounds.[32]

2.5.2. Toxicity Study. Finally, we utilized ProTox-II, a free website (https://tox-new.charite.de/protox_II/) to predict small molecule toxicity and to confirm whether the compounds would have a potential hepatotoxic impact.[33] The toxicity prediction captures issues such as oral toxicity, hepatotoxicity, mutagenicity, carcinogenicity, cytotoxicity, and immunotoxicity along with the metabolic pathways, inhibited by the molecule. The toxicity is determined in terms of LD50 (mg/kg body weight), and arranged as class 1: LD50 ≤ 5: fatal upon oral administration; class 2: 5 < LD50 ≤ 50: fatal upon oral administration; class 3: 50 < LD50 ≤ 300: toxic upon oral administration; class 4: 300 < LD50 ≤ 2000: harmful upon oral administration; class 5: 2000 < LD50 ≤ 5000: can be damaging upon oral administration; class 6: LD50 > 5000): nontoxic upon oral administration.[34]

2.6. *In Vitro* Cytotoxicity Data. The human foreskin fibroblasts (HFF) cell line was prepared from the Pasteur Institute of Iran, (Tehran, Iran). The cell line was grown in the DMEM medium, 10% FBS, 1% penicillin/streptomycin, and was incubated at 37 °C in the 5% CO$_2$ atmosphere. The antiproliferative activities of the AAs against the HFF cell line were specified *via* the MTT assay (3-(4,5-dimethylthiazol-2-yl)-2,5-diphenyltetrazolium bromide; Sigma-Aldrich, USA). The cytotoxic effects of the glycine were tested as a reference compound. The cell viability assay from the cytotoxicity effects of AAs was studied in a 96-well plate (1 × 10^4 cell/mL) and overnight adherence. Next, the HFF cell lines were incubated for 48 h with various doses of each AA (100−1000 μM). Specifically, 20 μL of MTT solution (5 mg/mL) was added to the cultured media for 3 h at 37 °C before the incubation finished, after which the insoluble formazan was formed. After the incubation, the supernatant obtained from each well was removed, and 200 μL of DMSO solution was added to the wells for solubilizing the formed formazan crystals. The concentration of compounds in half of the maximal inhibited growth is the IC$_{50}$ value employed in the cytotoxicity evaluation.[35] Ultimately, the optical density (OD) of dissolved insoluble formazan generated was measured at 590 nm using a multiwell scanning spectrometer. Data were analyzed using the GraphPad Prism VR 8.0.1.244 software (USA).

2.7. Experimental Binding Mode Study. In this study, all solutions were made just before they were used. For all experiments, stock solutions of DNA (5 mg/mL) and HSA (0.8 mg/mL) were produced in Tris−HCl buffer (including NaCl 10 mM, pH = 7.4) and stirred slowly at 4 °C until it becomes homogeneous. Both propylgly and 2-aminoheptylgly were dissolved in 5 mM stock solutions, which were diluted with double-distilled water. Electronic absorbance at 280 nm (280, HSA ε = 44,300 M^{-1} cm^{-1}) and 258 nm (258, DNA ε = 6600 M^{-1} cm^{-1}) were used to determine the true HSA and DNA concentrations, respectively.[36]

2.7.1. Experiments with UV−vis. UV−vis spectroscopy within the 200−400 nm region at RT was used to take the titration readings. The ligand stock solution (50 to 800 μL) was used to titrate 1.5 mL of DNA (0.064 mM) and HSA (0.01 mM) solutions. The UV pattern was determined by waiting 3 min for the solution to equilibrate after each addition. The apparent binding constant (K_{app}) for the biomolecule-AA can be calculated using eq 3 from the absorption data.

$$\frac{1}{A - A_0} = \frac{1}{A_\infty - A_0} + \frac{1}{K_{app}(A_\infty - A_0)} \times \frac{1}{[\text{compound}]}$$

$$(3)$$

A_0 and A are the absorbances of DNA (at 258 nm) or HSA (at 280 nm) in the absence and presence of ligand, respectively; A_∞ is the absorption when the biomolecule is saturated with the ligand solution, and [compound] represents the concentration of the AA derivatives. The K_{app} value is calculated by the ratio of the intercept to the slope of a linear association between the $1/(A - A_0)$ and $1/[\text{compound}]$ chart. The change in free energy ($\Delta G°$) was calculated using K_{app} values for DNA-/HSA-compound through formula 4.

$$\Delta G° = -RT \ln K_{app}$$

$$(4)$$

The ideal gas constant (1.9873 cal/mol·K) is represented by R, and the absolute temperature (300 K) is denoted by T. The value of $L_{1/2}$ can be found using a sigmoidal plot of A vs compound concentration (either going down or up).[37]

2.7.2. Fluorescence Investigation of AAs in DNA Binding. The binding modes of DNA in the interaction with propylgly and 2-aminoheptylgly, as small molecules, were investigated by the fluorescence emission monitoring DNA-EB system (the $\lambda_{excitation}$ was considered 471 nm). A solution containing 12×10^{-2} mM DNA incubated by 2×10^{-3} mM EB was titrated by various dosages of two candidate glycine derivatives (0 to 2.2 mM), and emissions were recorded at $\lambda_{emission}$ in the region of 540 and 700 nm (slit width: 10 nm) at room temperature.

2.7.3. Circular Dichroism Experiment. Circular dichroism is an optical method that can detect changes in the conformation of chiral biomacromolecules such as DNA and HSA, which are caused by interactions between them and drugs. A positive band at 273 nm suggests base stacking, whereas a negative band at 245 nm shows right-handed helicity in the B-DNA CD spectrum. The free HSA exhibits two minimum peaks, the first at 209 nm associated with $\pi-\pi^*$ transfer and the second at 220 nm attributed to n−π^* transition in the far-UV.[38] The CD spectra of HSA and DNA were obtained at concentrations of 8 $\times 10^{-4}$ mg/mL and 0.12 mM, with and without propylgly and 2-aminoheptylgly (0−24 mM). The measurements were carried out in a nitrogen environment at RT in Tris-buffer (including NaCl 10 mM, pH = 7.4) in the range of 200−320 nm for DNA systems and 176−260 nm for HSA systems using a cuvette cell (path length of 1 mm). All CD signals were first deducted for the background CD spectrum, then converted to molar ellipticity, and finally smoothed using CD software.

2.7.4. Viscosity Measurement. To determine viscosity values of propylgly and 2-aminoheptylgly in the interaction with ct-DNA, an Ostwald microviscometer was applied at room temperature. The ratios were considered ri = [AA]/[ct-DNA] = 0, 0.1, 0.2, 0.3, 0.4, 2, 4, 5.8, 7.6, and 10.8, and EB was used as intercalator reference. The flow time was defined five times for each sample using a digital timer, and the average

value was determined for viscosity measurements to be completed. The results were shown graphically as $(\eta/\eta_o)^{1/3}$ versus ratios, where η and η_o are related to viscosities of ct-DNA/AA solution and free ct-DNA, respectively, by applying the equation $\eta = (t - t_o)/t_o$, (t_o and t are the obtained flow times of free Tris-buffer and each DNA solution, respectively.[39]

2.8. Theoretical Docking Simulation. The molecular simulation method was used as an efficient way to predict the proper binding mode and hence the interaction region with DNA and HSA.[40] The three-dimensional crystal structures of DNA and HSA (PDB ID: 1BNA: 5′-D-(*CP*GP*CP*GP*AP*AP*TP*TP*CP*GP*CP*G)-3s′ and 1ao6) were taken from the Protein Data Bank (www.rcsb.org/pdb). These PDB files were converted to PDBQT, and the initial input files for AAs are generated from DFT optimization. Afterward, AAs were docked to DNA and HSA using AutoDock 1.5.6rc3 with AutoGrid 4.2.5, based on the Lamarckian genetic algorithm. A grid box of points in the x, y, and z directions were built and centered in the center of the compounds. The lowest docking binding energy conformation was chosen as the best binding mode concerning the AutoDock scoring function. Ultimately, the structure of each compound was created by the Chimera and the Discovery Studio (Version 1.15 an) software.[41]

3. RESULTS AND DISCUSSION

Nature has substituted a proton of glycine with different R groups and made 19 (+glycine) standard amino acids from which many proteins are synthesizable. Here, we report several N-substituted glycine derivatives (Scheme 1) via a green synthesis procedure. Each derivative contains an aliphatic and flexible R group, which can impose different properties on them. Due to selecting the long chain band for glycine derivatives with an R group, with more than three carbons in the chain, lipophilicity and solubility effects on the biological activity of synthesized glycine can be studied. Thus, the present work focuses on the effects of these R groups as well as N-substituted glycine derivatives as a whole, on their cytotoxicity, DNA, and HSA interaction properties. These studies include the characterization of derivatives, cytotoxicity, and detailed theoretical and experimental DNA/HSA binding studies, which are explained further.

3.1. FT-IR & FREQ-DFT. The infrared spectra of compounds were recorded within 4000−400 cm^{-1} as KBr pellet, and the maximum significant bands were as follows. The broad bands at 3500−3200 and 3100−2900 cm^{-1} are attributed to the O−H and N−H stretching vibrations, respectively.[42] The band at ∼2950 cm^{-1} is related to the CH stretching vibration of methyl and methylene groups. The strong absorption at 1760−1750 and 1420−1410 cm^{-1} is assigned to $\nu_{as}(COO^-)$ and $\nu_s(COO^-)$, respectively. The N−H bending vibrations of the amino group are particularly localized at approximately 1630−1550 cm^{-1}; however, there are a few overlaps within the range because of bending modes. The OH stretching frequency is unique to neutral glycine and its acid salt. The $\nu(OH)$ is shown as a distinct band at around 3500 cm^{-1} in the FT-IR spectra of neutral glycine. In contrast, the acidic form's band in this area is broad due to the effect of hydrogen bonding. Thus, the broadband illustrated an acidic version of AA derivatives in this article. On the other hand, the absence of the stretching frequency of COO$^-$ at 1650 cm^{-1}, which is related to the zwitterion, is another reason for the existence of the carboxylic acid.[43] The appearing peak at 1700

cm^{-1} in the IR spectra proves glycine derivative formation. Also, NMR data confirm the synthesis of different derivatives of glycine because the peak, related to the proton signal of CH$_2$ enclosed between two groups of NH$_2$ and COOH, has appeared at 3.5 to 4 ppm in ^{1}H NMR spectra and at 45 to 60 ppm in ^{13}C NMR spectra and also a peak at ∼160−170 ppm, which related to the C=O group in the amino acid derivative (see Figures S10−S20 in supporting information).[44] Figure 1
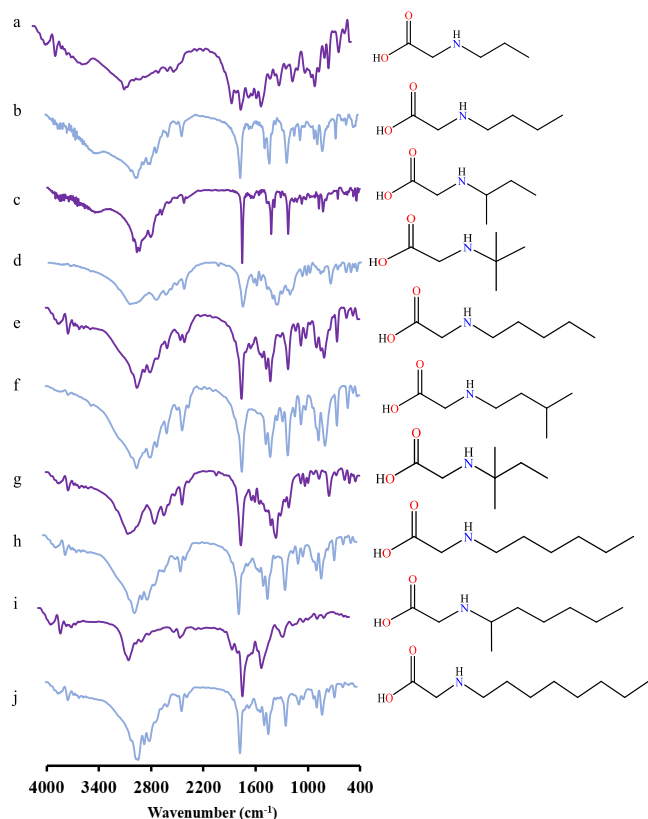
Figure 1. FT-IR spectra of amino acid derivatives (a) propylgly, (b) butylgly, (c) *sec*-butylgly, (d) *tert*-butylgly, (e) pentylgly, (f) isopentylgly, (g) *tert*-pentylgly, (h) hexylgly, (i) 2-aminoheptylgly, (j) octylgly.

displays the FT-IR spectra of all compounds. Since the Freq-DFT computational studies are the main idea for the validation of structures, the geometry of all AAs was optimized by the Opt-Freq keyword using the Gaussian tools.[33,34] The

comparison between simulated and experimental IR spectra is displayed in Figure S21. Some important vibration modes were identified, and their frequency is tabulated in Table S12. The results revealed a good agreement between the experimental and theoretical data obtained from DFT calculations.

3.2. DFT Calculations. *3.2.1. Molecular Geometry Analysis.* The molecular structure of all AAs was optimized using the Gaussian09 AML64-G09 Revision-D.01 program packages and Gauss view 6.0.16 tools. All compounds were also subjected to DFT calculations at the B3LYP/6-31g(d) level of theory.[26,27] Table 1 outlines the calculated QCDs in water: electronegativity, chemical hardness, softness, dipole moment, *etc.*, which show the trend of biological characteristics and molecular stability. In these studies, glycine is utilized as a reference. The highest occupied molecular orbital (HOMO) and the lowest unoccupied molecular orbital (LUMO) are the most important orbitals in a molecule. The E_{gen} values of HOMO and LUMO as well as the energy gap between HOMO−LUMO reflect the molecule's biological activity.[45] HOMO and LUMO calculations of ligands reveal that the electron density of HOMO is mostly localized on compounds except for the aliphatic branch. The charge distribution of the HOMO level in the case of ligands was highly centralized on the lone pair of N atoms of the AA group and the π^* charge of the carbonyl moiety. Furthermore, the charge distribution of the LUMO level was mostly delocalized over the carboxyl group with π^* antibonding feature and amino moieties of the ligand molecules. The computed quantum chemical parameters of the compounds are calculated using the following equations and shown in Table 2: ionization energy ($I = -E_{HOMO}$); electron affinity ($A = -E_{LUMO}$); absolute hardness ($\eta = -(E_{LUMO} - E_{HOMO}) / 2$); chemical softness ($\sigma = 1/\eta$); absolute electronegativity ($\chi = -(E_{LUMO} + E_{HOMO})/2$); chemical potential (CP $= -\chi$); electrophilicity index ($\omega = CP^2/2\eta$); global softness ($S = 1/2\eta$); nucleophilicity index ($N = 1/\omega$); additional electronic charges ($\Delta N_{max} = -CP/\eta$).[46,47] As the frontier orbital gap is small, the molecule is more polarizable, which means a high chemical reactivity as well as low kinetic stability. On the other hand, in the comparison of glycine to the structure octylgly and isopentylgly, with the increase of the hydrocarbon branch, it is observed that the energy gap has diminished from 6.68 for gly to 6.32 for isopentylgly, in response to which its biological activity would increase (see Figure 2). The other parameter is the negative chemical potential, which can be called absolute electro-

Table 1. Quantum Chemical Parameters Obtained for Amino Acid Derivatives

	gly	*tert*-butylgly	*tert*-pentylgly	*sec*-butylgly	2-aminoheptylgly	propylgly	butylgly	pentylgly	hexylgly	octylgly	isopentylgly
$E_{HOMO}{}^a$	−6.51114	−6.02352	−5.98433	−6.05943	−5.95059	−6.00746	−5.99413	−5.98814	−5.98351	−5.98025	−5.97671
$E_{LUMO}{}^a$	0.168983	0.401096	0.408443	0.324632	0.416334	0.345313	0.347762	0.349666	0.35402	0.353204	0.34857
$\Delta E_{gap}{}^a$	6.680127	6.424612	6.392774	6.384067	6.366923	6.352773	6.341889	6.337807	6.337535	6.333453	6.32529
η^a	3.340063	3.212306	3.196387	3.192033	3.183462	3.176387	3.170944	3.168904	3.168768	3.166727	3.162645
σ^b	0.299396	0.311303	0.312853	0.31328	0.314123	0.314823	0.315363	0.315567	0.31558	0.315783	0.316191
χ^a	3.17108	2.81121	2.787944	2.867401	2.767127	2.831074	2.823183	2.819237	2.814747	2.813523	2.814067
CP^a	−3.17108	−2.81121	−2.78794	−2.8674	−2.76713	−2.83107	−2.82318	−2.81924	−2.81475	−2.81352	−2.81407
ω^a	1.505323	1.230098	1.215846	1.287892	1.202621	1.261651	1.25678	1.254077	1.250139	1.249857	1.251954
N^a	0.664309	0.812944	0.822472	0.776462	0.831517	0.792612	0.795684	0.797399	0.799911	0.800092	0.798751
ΔN_{max}	0.949407	0.875138	0.872217	0.898299	0.86922	0.891288	0.890329	0.889657	0.888278	0.888464	0.889783
S^b	0.149698	0.155651	0.156427	0.15664	0.157062	0.157412	0.157682	0.157783	0.15779	0.157892	0.158096

^{a}In eV. ^{b}In eV^{-1}.

Table 2. Lipophilicity and Solubility Values of the AA Derivatives from Experimental and Theoretical (ADME) Methods

compound	experimental log$P$	theoretical log$P$	solubility in water g/mL	experimental log$S$	theoretical log$S$
Gly	−2.76	−3.21	2.1 ± 0.18	0.32	0.83
propylgly	−1.85	−2	0.31 ± 0.03	−0.50	−0.85
tert-butylgly	−1.91	−1.77	0.2 ± 0.01	−0.69	−0.88
butylgly	−1.97	−1.64	0.12 ± 0.02	−0.89	−1.28
sec-butylgly	−1.47	−1.56	0.11 ± 0.03	−0.93	−0.9
tert-pentylgly	−1.28	−1.24	0.32 ± 0.01	−0.48	−1.3
isopentylgly	−1.13	−1.2	0.26 ± 0.01	−0.57	−1.32
pentylgly	−1.27	−1.1	0.39 ± 0.00	−0.40	−1.69
hexylgly	−0.89	−0.55	0.16 ± 0.00	−0.79	−2.11
2-aminoheptylgly	−0.17	−0.12	0.09 ± 0.00	−1.00	−2.15
octylgly	0.24	0.53	0.01 ± 0.01	−1.94	−2.93
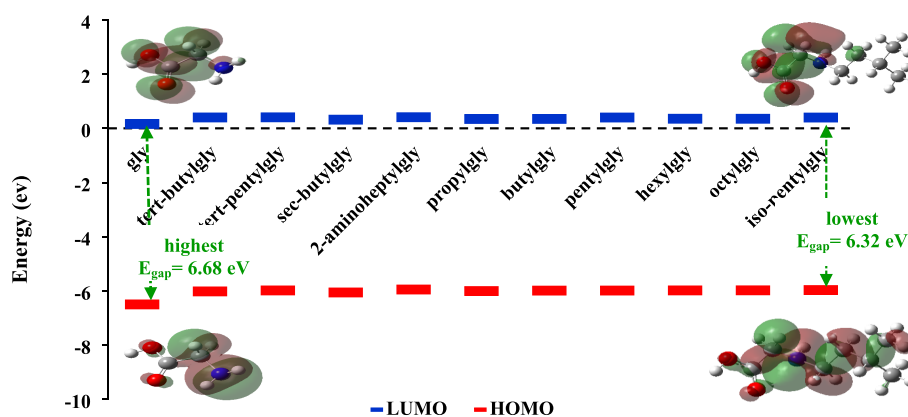
Figure 2. Homo and LUMO energy schematic for AA (gly with the highest E_{gap} = 6.68 eV and isopentyl with the lowest E_{gap} = 6.32 eV).

negativity, and it means a transfer of electrons from a less electronegative system to a more electronegative system. Small values of global electronegativity signify that electrons were delocalized on the molecule and so the molecule can easily give electrons to coordinate appropriate structure, so bioactivity has increased. In the comparison of glycine (3.17 eV) to the bulky compounds, it is observed that electronegativity has decreased especially for 2-aminoheptylgly with the lowest value (2.76 eV), and biological activity increases. The surface plots of HOMO and LUMO are shown in Figure 2 for all AA derivatives.

3.2.2. MEP Simulation and TD-DFT Determination. In the following, 3D plots of MEP, molecular electrostatic potential of studied compounds, have been drawn at the water phase to better understand the electronic density on the molecular surface as well as describe the reactive sites for electrophilic and nucleophilic reactions as along with hydrogen bonding interactions (see Figure 3). The negative electrostatic potential corresponds to an attraction of the proton by the concentrated electron density in the molecule (red color). The positive electrostatic potential corresponds to the repulsion of the proton by atomic nuclei in regions where low electron density exists and the nuclear charge is incompletely shielded (blue color). The importance of MEP lies in the fact that it simultaneously displays molecular size and shape as well as charges electrostatic potential regions in terms of color grading. The potential grows in the order red < orange < yellow < green < blue.[46] As seen from the MEP map, the regions with a positive potential (blue) are mostly the hydrogen atoms of amino and carboxyl groups, especially in bulky glycine derivatives. This kind of hydrogen provides hydrogen binding for nucleophile groups, such as DNA base

pairs, which leads to the formation and stability of adducts (DNA-ligand). Meanwhile, the orange-red areas that have a negative electrostatic potential are over the oxygen atoms in the carboxyl group. A similar observation has been reported for cyclohexyl glycine.[48] Related data show its strong tendency to connect with DNA is dependent on electron-deficient species on carboxylate and amine sections of glycine structure.[48] These regions are related to nucleophilic reactions that lead to electron transfer to Lewis acids such as metal ions. Dipole moment calculation ($\mu\rightarrow$) is obtained by computing the TD-DFT, which showed that propylgly with the highest value is 2.13 Debye and 2-aminoheptylgly with the lowest value is 1.09 Debye.

3.3. Solubility and Lipophilicity Measurements. The solubility and lipophilicity of a compound play significant roles in cellular accumulation and oral bioavailability in drug development.[49] The lipophilicity and solubility of the AA derivatives have been conducted *via* the shake flask and saturated aqueous solution procedure, respectively, and all data are listed in Table 2. Experimental data collection shows that solubility values decrease from gly to octylgly (log$S$ = 0.32 to −1.94), though all of them are very soluble. On the contrary, lipophilicity was increased from gly (log$P$ = −2.76) to octylgly (log$P$ = 0.24). As Figure 4a depicts, the amount of solubility has a downward trend, but all of them are in the good range of solubility based on ADME (SILICOS-IT) theory calculations.[32] Meanwhile, lipophilicity is a significant physiological characteristic to evaluate a drug's capacity to cross over cell membranes, and this trait may affect the cytotoxicity activity of synthesized complexes.[31] The phospholipid portion of cell membranes can easily permeate lipophilic compounds to penetrate across it. A basic pharmacokinetic index, known as
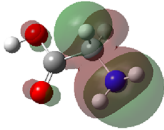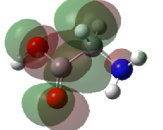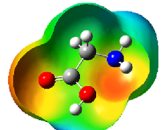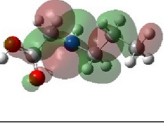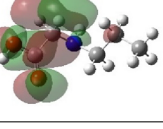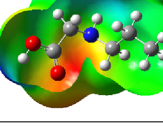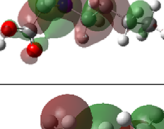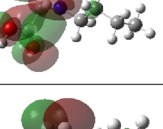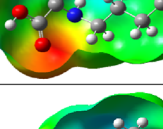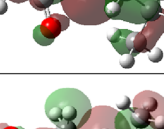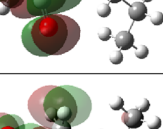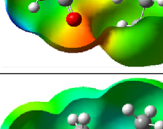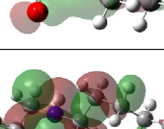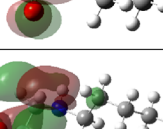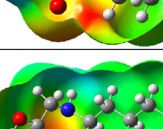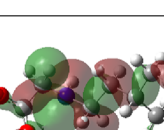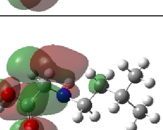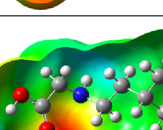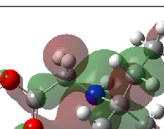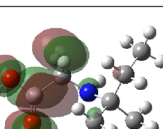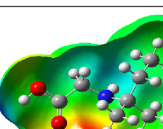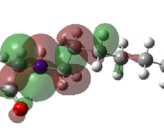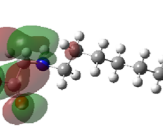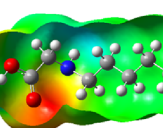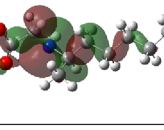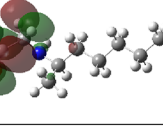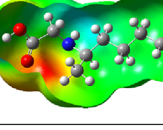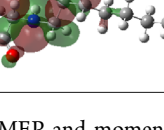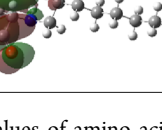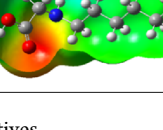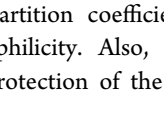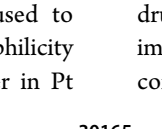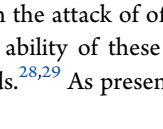
	HOMO	LUMO	MEP	$\vec{\mu}$ (Debye)
gly				1.38
propylgly				2.13
butylgly				1.36
sec-butylgly				1.27
tert-butylgly				1.38
pentylgly				1.41
iso-pentylgly				1.38
tert-pentylgly				1.36
hexylgly				1.42
2-aminoheptylgly				1.09
octylgly				2.09

Figure 3. HOMO−LUMO and MEP and moment dipole values of amino acid derivatives.

the logP (water/n-octanol partition coefficient), is used to assess the compound's lipophilicity. Also, the lipophilicity property may facilitate the protection of the Pt center in Pt

drugs from the attack of off-target biological nucleophiles as an important ability of these ligands in the structure of their Pt compounds.[28,29] As presented in Figure 4b, logP is determined
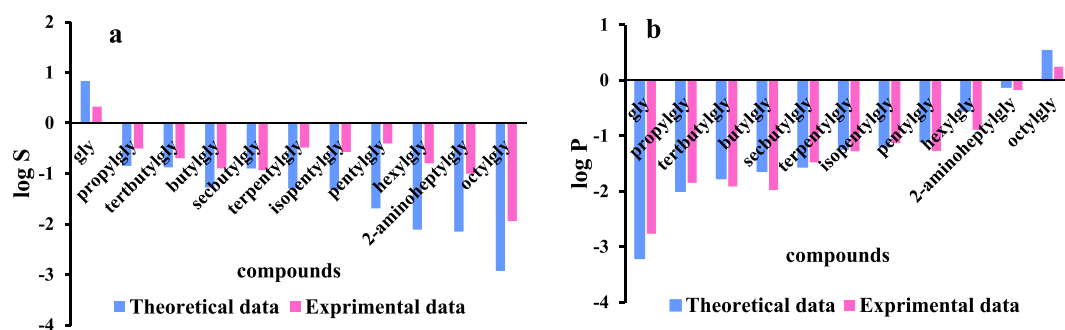
Figure 4. Exp. and calc. data of solubility (a) and lipophilicity (b) of AAs.
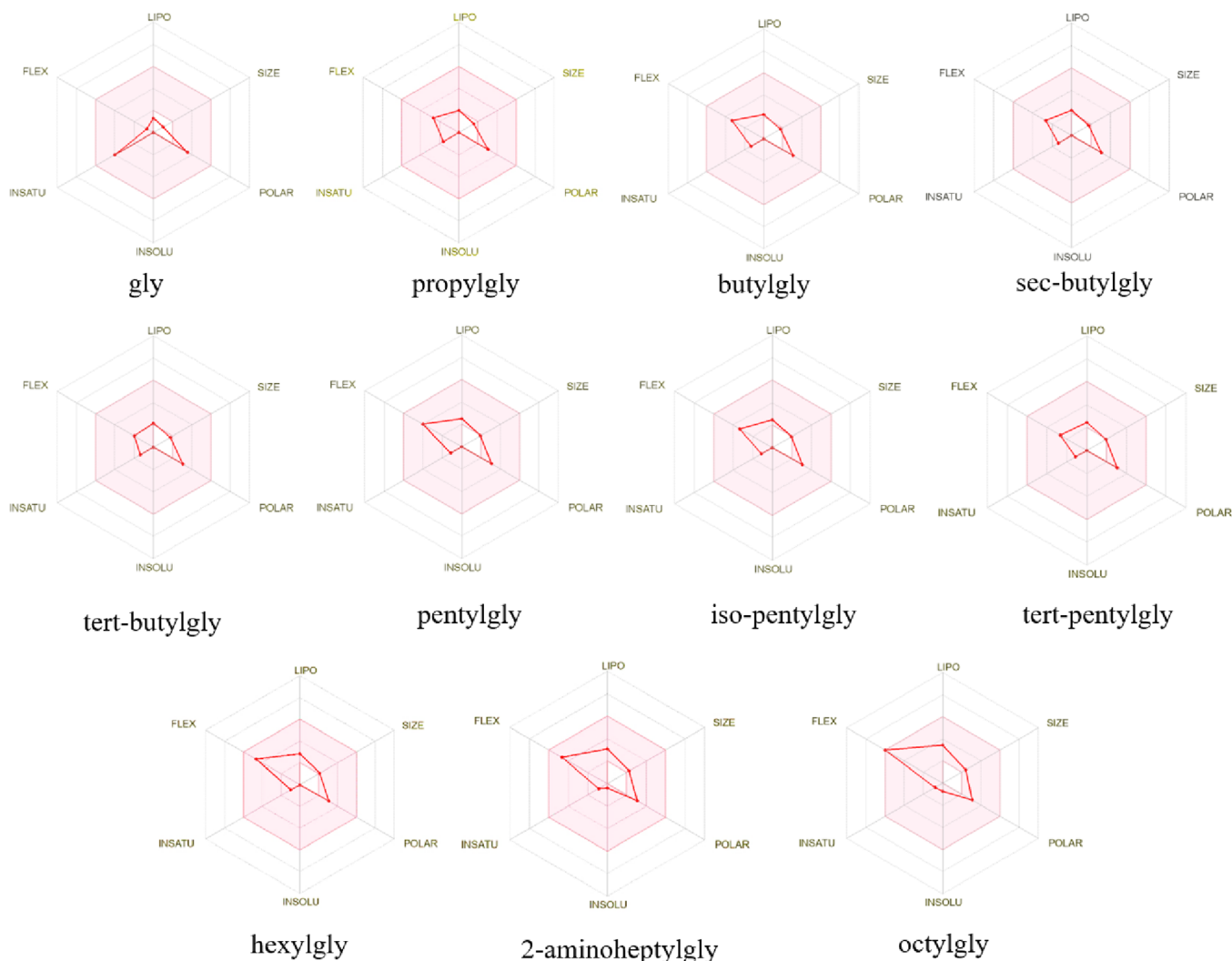
Figure 5. Bioavailability radar as drug-likeness for AA derivatives.

for the above AA derivatives and compared with calculated data obtained from ADME (XLOGP3). As amine and carboxylate moieties are contained in all of these compounds, different relative $clogP$ (calculated logarithm of partition coefficient) values should depend on the length of the hydrocarbon chain derivatives. This indicates that upon increasing hydrocarbon chain length or branches, lipophilicity would grow as well. All measurements were repeated three times.

3.4. Pharmaceutical Activities. *3.4.1. Drug-Likeness Analysis.* Nowadays, ADME is one of the initial prediction tools in pharmaceutical research and advancement. This prediction guides researchers toward drug efficiency and potency and provides insights into whether or not the studied compounds have properties as orally active drugs. This prediction relies on an already established theory by Lipinski et al., named Lipinski's rule of five.[50] For a molecule that is a candidate for active medication, no more than one rule should be disregarded. These rules are the number of hydrogen bond

Table 3. Cytotoxicity Values of Compounds against the HFF Cell Line for 48 h

AA	IC$_{50}$ (μM) ± SD
gly	252.5 ± 16.5
propylgly	314.8 ± 11.8
butylgly	239.1 ± 28.5
sec-butylgly	252.7 ± 22.5
tert-butylgly	250.3 ± 15.1
pentylgly	243.2 ± 3.9
iso-pentylgly	231.8 ± 24.2
tert-pentylgly	177.6 ± 24.4
hexylgly	290.2 ± 8.8
2-aminoheptylgly	127.5 ± 20.9
octylgly	344.8 ± 18.5
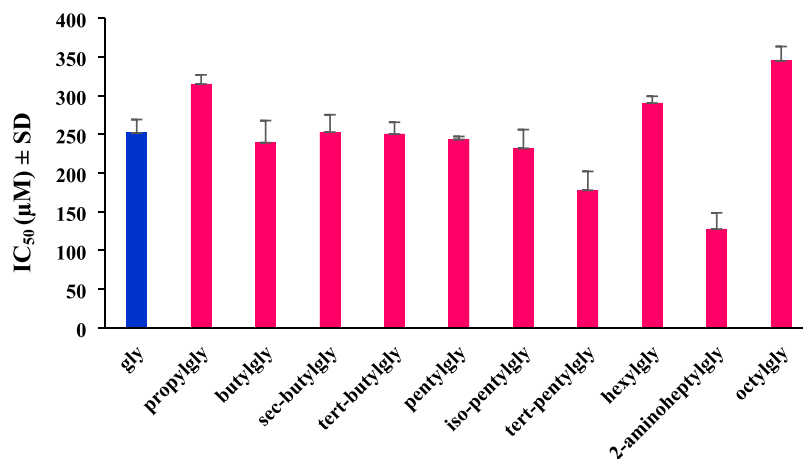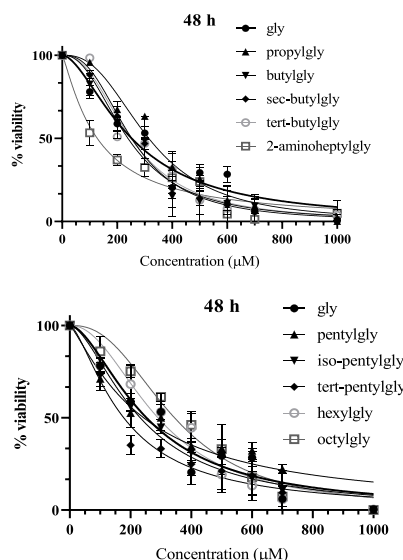
Figure 6. IC$_{50}$ values (μM) of AAs on HFF cells after 48 h. The results are presented as mean ± SD.

acceptors (≤10), number of hydrogen bond donors (≤5), molecular weight (Mw: 150−500), logarithm of the projected octanol−water partition coefficient (clogP_o/w: −2 to 6.5), and topological polar surface area (TPSA: 20−130).[25,42] The chemical structure of components was converted to their SMILE type and submitted to the SwissADME software to estimate in silico pharmacokinetic parameters. As observed in Table S13 in the Supporting Information, all compounds had acceptable drug-like rules. For propylgly to octylgly, the clog$P$ is within −2 to 0.53, with mass values of 117.15 to 187.28 g/mol, where the number of hydrogen donors and acceptors is less than 5 and 10, respectively. Also, TPSA (topological polar surface area) is 49.33 Å^2, which is in the acceptable range (7.0−200.0), and all synthesized compounds comply with Lipinski's five laws. One of the important items in the table is the value of clog$P$ or lipophilicity, which shows that with the increase of the hydrocarbon branch, lipophilicity has grown, which can suggest usefulness of these AAs in the design and synthesis of oral drugs.

The bioavailability radar shows a rapid overview of several physicochemical aspects. The pink area indicates the best area for all compounds from gly to octylgly. In addition to Lipinski's

law, other factors in this radar include the solubility of log$S$ ≤ 6, amount of sp^3 hybridization of carbon ≥0.25, and flexibility ≤ 9. Also, the experimental method for lipophilicity and solubility revealed that the range of log$S$ and log$P$ lay within 0.3 and −2.7 for gly to −1.9 and 0.24 for octylgly, respectively.[50] As described, all compounds are entirely in the pink area, so they can be considered drug-like compounds (see Figure 5).

Figure S22 displays the BOILED-Egg model, which operates by calculating various features of a medication candidate. It has two spaces, white and yellow, which indicate locations with the greatest chance of percolating to the blood−brain barrier (BBB) and gastric absorption intake (GI Abs.), respectively. Also, compounds with blue dots would be substrate and they are actively emanated by P-glycoprotein (PGP+), but other compounds are (PGP−) and red dots. The permeability of the components through the BBB indicated that they can be practicable in treating inflammation.[51] The prediction indicated that five compounds of gly, propylgly, butylgly, sec-butylgly, and tert-butylgly are in the white region of the egg. They are absorbed by digestion, but they do not penetrate the brain. Other compounds are in the yellow region, which passes
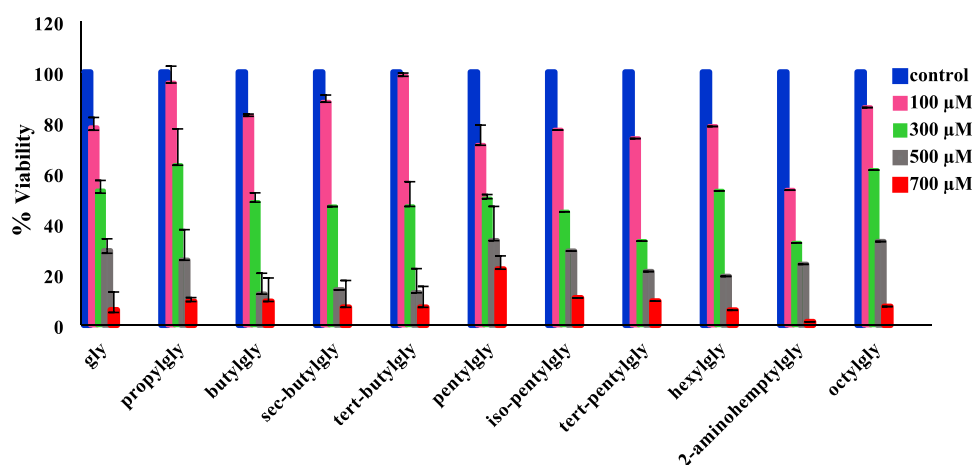
Figure 7. Cell viability percentage of all compounds against the HFF cell line.
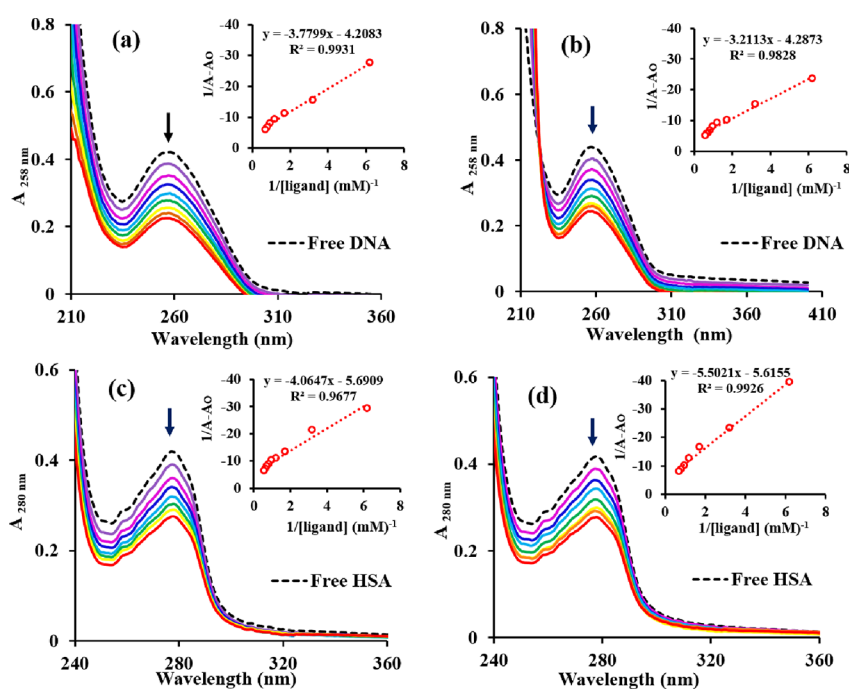

Figure 8. UV−vis monitoring of DNA ((a) propylgly, (b) 2-aminoheptylgly) HSA ((c) propylgly, (d) 2-aminoheptylgly) in Tris−HCl buffer at pH = 7.4. The arrow illustrates the direction of alteration in intensity upon increasing the concentration of the AA. K_{app} for DNA and HSA binding obtained by plotting $(1/A − A_0)$ versus $1/[\text{compound}]$.

through the blood−brain barrier and is not pumped out due to the red color of the PGP− points. Based on data in Table S13, all compounds have high intestinal absorption (GI Ads.)

3.4.2. Toxicity Study. The toxicological prediction offers effects of endpoints, such as hepatotoxicity, carcinogenicity, mutagenicity, immunogenicity, and cytotoxicity. However, propylgly, butylgly, pentylgly, hexylgly, and octylgly have proven to induce carcinogenicity.[52] As glycine is one of the most widely used amino acids in plant nutrition,[53] and cancers occur due to any changes in cell division and normal biological processes, these above derivatives can be substituted for glycine in carcinogenetic and chemotherapy *in vivo* studies.[54] Pro-Tox II is a virtual lab for predicting the toxicities of small molecules. Based on the above result prediction analysis, presented in Table S14, none of the compounds has shown acute toxicity and may be probably tested as a true drug candidate.

3.5. Cytotoxicity Activity. The cytotoxicity of the synthesized AAs was evaluated via the MTT assay to determine the anti-proliferative property against the HFF cell line with the IC_{50} values listed in Table 3. IC_{50} values of all compounds were obtained at the different dosages of each AA against HFF after 48 h, and glycine was considered as a reference agent (see Figure 6).

2-Aminoheptylgly and octylgly revealed the lowest (127.5 μM) and highest (344.8 μM) values, respectively. The results showed that all compounds have no significant toxicity against the HFF cell line. However, it seems that the inhibitory effect of the 2-aminoheptylgly is more potent than that of all compounds after 48 h. On the other hand, for similar derivatives, the IC_{50} value was reported $\geq$700 μM against several anticancer cell lines.[40] Figure 7 indicates the cell viability, which is the growth percentages estimated as the

absorbance of the treated cells/absorbance of the control cells × 100 (%).[55]

3.6. DNA- and HSA-Glycine Derivative Binding.

3.6.1. UV−vis Study. Electronic absorption monitoring can be used as a fundamental tool for studying the binding propensity of substances to biomacromolecules.[56] Figure 8 illustrates the absorption spectra of DNA and HSA titrated with different volumes of two candidate AA, propylgly with small and 2-aminoheptylgly with a bulky hydrocarbon chain, (100 to 800 μL from ligand stock solution for DNA and 100 to 700 μL for HSA, respectively). The peak intensity of DNA and HSA drops as AA concentration rises. This demonstrates a kind of conformational change that occurs in these biomolecules' fundamental structures in response to ligand binding. This is because the UV-absorbing components of DNA and HSA are obscured during refolding, leading to hypochromicity or a reduction in absorption intensity.

The following formula 5 is used to achieve a rough approximation of the hypochromicity:

$$H\% = \frac{A_{\text{free}} - A_{\text{bounded}}}{A_{\text{free}}} \times 100 \qquad (5)$$

K_{app} was computed using the titration data to more accurately estimate the magnitude of the compounds' binding strengths to DNA and HSA. The K_{app} values show that the interaction between these AAs and macromolecules is weak. Further, the $\Delta G°$ of compounds and biomolecules can be approximated using the equation $\Delta G° = -RT\ln K_{\text{app}}$. The negative value of $\Delta G°$ shows the spontaneous binding.[57] The obtained free energy and other calculated data are tabulated in Table 4. The low K_{app} value for binding results in the reversible

Table 4. Data Obtained from UV−vis Studies for the Interaction of the AAs with DNA/HSA at Room Temperature

	compound	K_{app} (mM^{-1})	$\Delta G°$ (kJ/mol)	H (%)	$[L]^{1/_2}$ (μM)
DNA binding	propylgly	1.11	−0.25	45.4	952
	2-aminoheptylgly	1.33	−0.70	44.5	794
HSA binding	propylgly	1.40	−0.82	38.3	781
	2-aminoheptylgly	1.02	−0.05	33.9	705

binding of compounds with HSA, which facilitates their safe delivery through circulation. On the other hand, a higher binding constant (K_{app}) for the interaction of the 2-aminoheptylgly with DNA than for propylgly suggests that its binding is stronger. This ability to construct a stable ensemble using biomacromolecules might be useful in drug design as a ligand in metal complexation. In a recent report,[13] the K_{app} and $[L]^{1/_2}$ values have been summarized in a review article for several Pt and Pd complexes in the interaction with DNA, which indicates that when these kinds of ligands were used in complexation, $[L]^{1/_2}$ values decrease about 10 times and K_{app} values of DNA-complex formation increase.[13,58]

Next, the AA dosage to unfold the biomolecule at the midpoint ($[L]_{1/2}$) parameter was determined, which represents the compound concentration at the midpoint of a biomolecule transition from the initial structure to the distorted shape. For plotting the graphs, the profile of alterations in the patterns of absorbance at 258/280 nm for DNA/HSA was plotted versus the concentrations of the targeted ligands (Figure S23). The concentrations of propylgly and 2-aminoheptylgly at the transition midpoint, $[L]_{1/2}$, have been 952 and 794 μM for DNA binding and 781 and 705 μM for HSA binding, respectively. Thus, in very high quantities, these components denature DNA or HSA. This suggests that if they are used as ligands in drugs designed to treat cancer, they may not have any adverse effects. This is in good agreement with cytotoxic data extracted from Pro-Tox II property explorer, presented in Table S14, which displays that these compounds are not cytotoxic.

3.6.2. Emission Monitoring. Emission spectra of DNA incubated by EtBr with both mentioned AA titration at 25 °C are presented in Figure 9. The Stern−Volmer equation ($F_o/F = 1 + K_{\text{sv}}[Q] = 1 + k_q\tau_o[Q]$) was used to ascertain how fluorescence is quenched.[59] F_o and F are the fluorescence intensities of EB-DNA before and after each titrating of the quencher, respectively ([AA] is $[Q]$). The fluorophore's unquenched lifespan (τ_o) is around 10^{-8} s, and k_q ($k_q = K_{\text{sv}}/\tau_o$) is the bimolecular quenching rate constant. K_{sv} is the Stern−Volmer quenching constant determined from a linear F_o/F vs $[Q]$ plot for propylgly and 2-aminoheptylgly (insert plots in Figure 9). K_{sv} values calculated from the Stern−Volmer quenching were found to be 0.42×10^3 and 0.28×10^3 M^{-1} for DNA-propylgly and DNA-2-aminoheptylgly systems. The values of k_q for synthetic compounds were more than the maximum dynamic quenching constant (2×10^{10} M^{1}s^1),
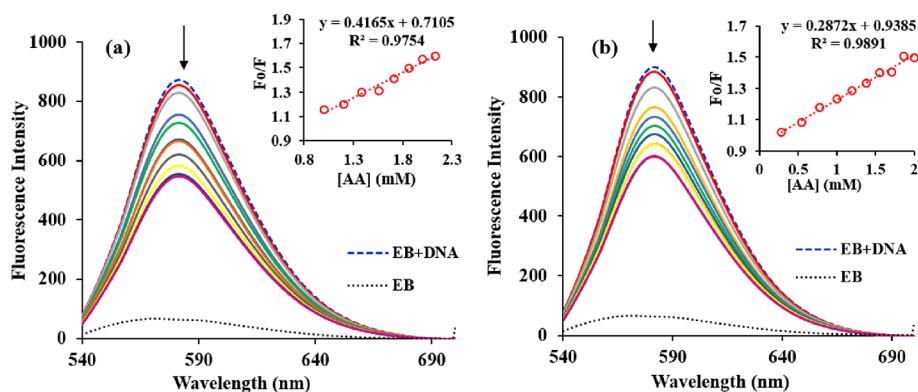

Figure 9. Emission monitored of DNA (0.12 mM) incubated by EtBr (0.002 mM) titration by propylgly (a) and 2-aminoheptylgly (b) (0 to 2 mM) at 25 °C; inset: related Stern−Volmer plots.
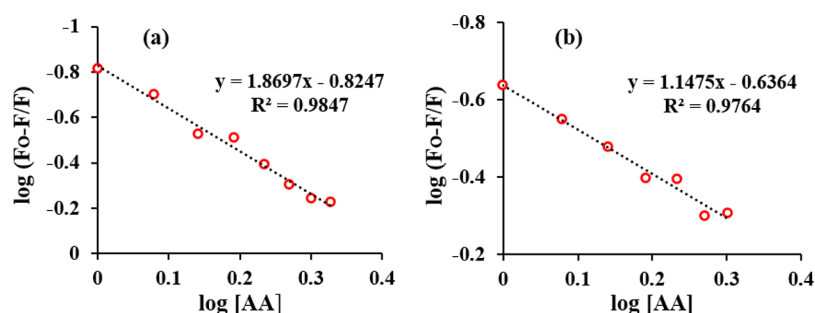
Figure 10. Plots of $\log(F_o - F/F)$ versus $\log[Q]$ of propylgly (a) and 2-aminoheptylgly (b) in interaction with ct-DNA.

Table 5. Binding Parameters of Propylgly-DNA and 2-Aminoheptylgly-DNA at Room Temperature[a]

compound	K_{sv} (M^{-1})	k_q $(M^{-1}\,s^{-1})$	R^2	K_b (M^{-1})	n	R^2
propylgly	0.42×10^3	0.42×10^{11}	0.97	0.15×10^3	1.87	0.98
2-aminoheptylgly	0.28×10^3	0.28×10^{11}	0.98	0.23×10^3	1.14	0.97
CHgly[40]	1×10^3	1×10^{11}	0.99	0.43×10^3	0.58	0.99

[a] R^2 is the correlation coefficient.

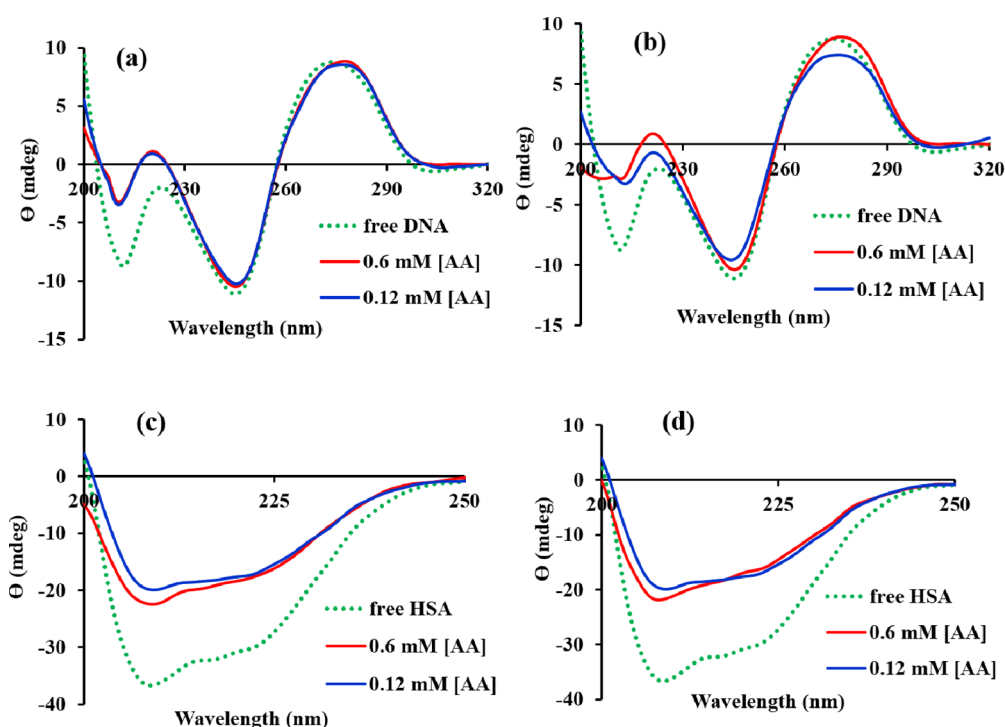**Figure 11.** CD spectral profiles of DNA ((a) propylgly, (b) 2-aminoheptylgly) (0.12 mM) and HSA ((c) propylgly, (d) 2-aminoheptylgly) (8×10^{-4} mg/mL) at pH = 7.4 and *RT* with increasing (0.60 and 0.12 mM) AA, respectively.

indicating that static quenching occurs. For the static quenching process, the equation $(\log(F_O - F/F) = \log K_b + n\log[Q])$[60] was used (as shown in Figure 10) to evaluate the binding constant, K_b, and the binding sites, n, to quantitatively examine the complex's capacity to bind DNA, whose data are listed in Table 5. K_b were 0.15 and 0.23 M^{-1} and n were 1.87 and 1.15 for the propylgly and 2-aminoheptylgly systems, respectively. These binding constants are lower than classical intercalative binding mode, so, groove binding can be considered for these mentioned glycine derivatives. Recently, the binding parameters reported[48] for cyclohexyl glycine (CHgly), as a cyclic aliphatic derivative of glycine, are K_b = 0.43 M^{-1} and n = 0.6, which indicates probably that cyclic aliphatic alkyl in the glycine structure leads to more affinity to

DNA binding because of the global symmetric structure created.

3.6.3. CD Spectroscopy Analysis. Circular Dichroism (CD) is a unique spectroscopic technique to clarify conformational changes of biomacromolecules when they bind to compounds. Hence, shifts in the location and strength of the spectral bands present certain information about interactions between macromolecules and compounds.[61] Figure 11 illustrates the CD spectra of DNA (0.12 mM) and HSA (8×10^{-4} mg/mL) in the absence and presence of the AAs (concentration of 0.60−0.12 mM).

According to Figure 11a,b, there is no change in the positive and negative bands for propylgly, showing that this AA has no specific effect on the DNA. On the other hand, the reduction

in intensity across both positive and negative bands for 2-aminoheptylgly can be observed, which displays its binding to B-DNA via weak electrostatic interaction. In addition, CD monitoring of DNA-cyclohexyl glycine solution shows the weak interaction and conformational modification in the DNA structure probably via electrostatic and groove binding.[48]

In protein titration, as shown in Figure 11c,d, the negative bands increase strongly without a significant shift. This shows that the reduction of the alpha-helix content in the protein and the binding of AAs to HSA cause the loss of stability of the helix of the second structure of the protein. According to Table 6, the amount of α-Helix, turn, and random coil has decreased for both AA-HSA systems, but β-sheet has increased for propylgly and decreased for the 2-aminoheptylgly system.

Table 6. Values and Relative Percentage of Secondary Structure Elements of HSA in the Presence of Propylgly and 2-Aminoheptylgly

	%α-Helix	%β-sheet	turn	%random coil
free HSA	61	11	3.8	24.2
propylgly (0.6 mM)	44.9	15.3	7.1	32.8
propylgly (0.12 mM)	41.3	17.3	7.4	34
2-aminoheptylgly (0.6 mM)	52.6	5.2	8.6	33.6
2-aminoheptylgly (0.12 mM)	49.3	8.2	9.4	33.1

3.6.4. Hydrodynamic Experiment. Hydrodynamic viscosity measurement is an effective tool to prove the binding mode of compounds with DNA. Due to the intercalation mode, DNA helical lengthens and viscosity increases, while during compound interaction with DNA through minor or major grooves, minimal or nonexistent changes appear in DNA viscosity.[62] The changes in the viscosity determined by DNA-AA solutions are presented in Figure 12 for both propylgly and 2-aminoheptylgly as well as EB[63] as a well-known DNA intercalator controller agent.
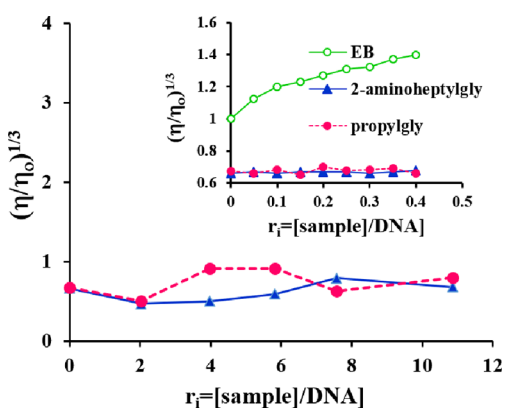

Figure 12. Viscosity changing of DNA by titrating different concentrations of AA compounds; inset plot: EB was used as an intercalator agent.

Figure 12 and the inset plot illustrate that when AAs were added to ct-DNA, no significant changes were noticed in viscosity progress and grove binding more probably occurs for both mentioned systems. To investigate the effects of them in high concentrations, measurement was continued up to ri of about 10 for each AA system. Considering spectroscopic analysis (UV−vis, CD, and fluorescence data), the interaction

of these compounds with DNA is the electrostatic type, and viscosity data confirms it is groove binding as reported in the docking study.

3.7. Docking Study. Molecular docking studies have a major role in structural molecular biology and drug discovery. To investigate the binding affinity of synthesized compounds with DNA/HSA, docking study was done to follow the relationship between chemical structure and biological activity. All synthesized compounds were subjected to molecular docking studied through AutoDock probed against (PDB ID: 1Bna) and human serum albumin proteins (PDB ID: 1ao6). The lowest energy should be considered to increase the precision of the binding mode in the system. The 200-cluster ranks were calculated, and the thermodynamic parameters results are presented in Tables S14 and S15 based on their energies for DNA and HSA binding, respectively. Tables S16 and S17 indicate that the primary rank is the most probable docking site due to its higher cluster rank, and we solely considered four free energies of the first rank for DNA and HSA binding, respectively. The expanded binding sites of all compounds to DNA/HSA are shown in Figures S24 and S25, respectively, in the lowest energy rank for all glycine derivatives. The negative energy predicts a moderate interaction between compounds and macromolecules. The results showed the cluster energy of octylgly is more negative (−5.55 kcal/mol) than gly (−3.48 kcal/mol), so the DNA-binding affinity of this AA is stronger than that of the others. This could be related to the increase of the hydrocarbon branch and suitable placement of this compound in biomolecule active sites in comparison to smaller structures. These obtained data are useful to provide insights into the designing and following effective anticancer agents.[64] To clarify how propylgly and 2-aminoheptylgly can be located within proper groove sites on DNA, Figure 13 is presented to show the existence of hydrogen and hydrophobic interactions. As shown in Figure 13, there are π-alkyl interactions between hydrocarbon chain and hydrogen binding between the functional group of ligand and helix of DNA. ΔG° of the 2-aminoheptylgly-DNA was obtained at −5.54 kcal/mol, which is more stable than the propylgly-DNA system (−4.18 kcal/mol). These results are in good agreement with the obtained UV−vis data (−0.7 and −0.25 kJ/mol for 2-aminoheptylgly and propylgly, respectively) and also K_b determined from the fluorescence study. This study has been performed for cyclohexyl glycine[48] and tertpentyl glycine[65] compounds that reported energy values of −5.71 and −6.49 kcal/mol, respectively, which means that their DNA interactions proceed via electrostatic force and groove binding interactions.

The result for HSA binding of all compounds showed that each AA has a special binding site except for pentylgly and isopentylgly, which have the same site. The most negative value of docking energy in all conditions shows a higher tendency of *tert*-pentylgly (−4.5 kcal/mol) for binding to HSA. Possibly, since it is small and has a highly symmetrical structure in its branch, it can penetrate HSA while others cannot. Based on previous reports, these values decreased to approximately −11 when the glycine coordinated with the metal ion as a ligand.[48,66] All interactions such as hydrogen bonds, carbon−hydrogen bonds, alkyl bonds, *etc.* are listed in Tables S18 and S19. The potential interaction sites for propylgly and 2-aminoheptylgly on HSA are shown in Figure 14. Unlike DNA interaction ΔG° of propylgly-HSA formation (−4 kcal/mol) was more negative than 2-aminoheptylgly
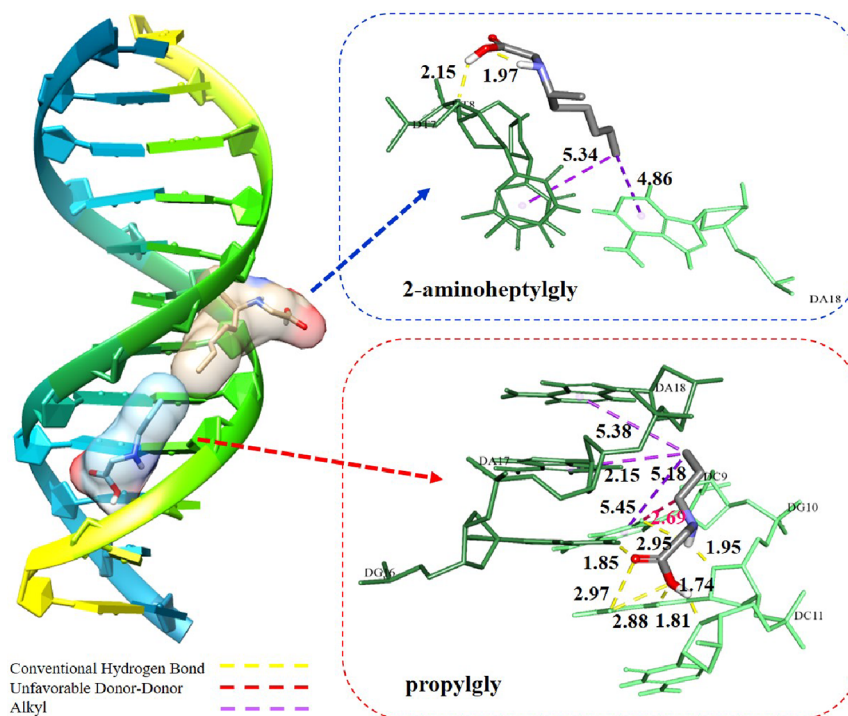
Figure 13. Docking pose of propylgly and 2-aminoheptylgly interaction with DNA.
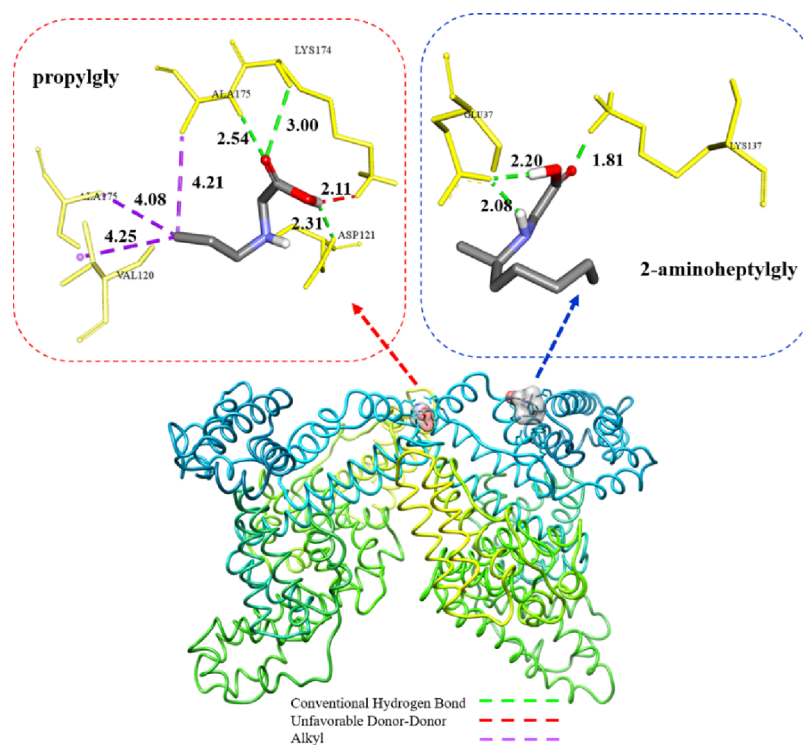
Figure 14. Docking pose of propylgly and 2-aminoheptylgly interaction with HSA.

(−3.61 kcal/mol), which is in agreement with the obtained $\Delta G°$ from UV−vis monitoring (−0.82 kJ/mol for propylgly and −0.05 kJ/mol for 2-aminoheptylgly) in HSA interaction. The values of electrostatic energies were evaluated to be more than vdW + Hbond + desolve, demonstrating that electrostatic attraction plays a vital function role in the HSA-interaction process. As shown in Figure 14, propylgly interacts with Lys174, Val120, Ala175, and Asp121 and 2-aminoheptylgly

interacts with Glu37 and Lys137 of the HSA residues. Alkyl interactions are also observed in the propyl composition, which is not present in 2-aminoheptylgly.

4. CONCLUSIONS

This study presented a green strategy with fewer steps than previous research to synthesize 10 aliphatic glycine derivatives as propylgly, butylgly, *sec*-butylgly, *tert*-butylgly, pentylgly,

isopentylgly, *tert*-pentylgly, hexylgly, 2-aminoheptylgly, and octylgly. They were specified by spectral IR, mass, ^{1}H NMR, and ^{13}C NMR data. To determine the molecular geometry, DFT and MEP analyses were done and data showed that the dipole moments ($\vec{\mu}$) are 2.13 to 1.09 Debye for propylgly and 2-aminoheptylgly with the highest and lowest values, respectively. In addition, the electron density investigation of the whole R-glycine structures displays that the negative electrostatic potential is over the oxygen atoms in the carboxyl group. According to these data, to approach and interact R-glycines with DNA or HSA, carboxyl section is the proper site on compound structures to play the role their biological properties. Also, the lipophilicity of all compounds was determined in terms of log$P$ and the obtained values lay within −2.76 for gly to 0.24 for octylgly. This indicated that the increase of the hydrocarbon branch can enhance the lipophilicity of the compounds.

Theoretical ADME and toxicity studies were done on these compounds to predict their bioactivities. Investigating the cytotoxic effect of AAs against the normal HFF cell line revealed that all compounds have a near cytotoxic activity to glycine; however, it seemed that the inhibitory effect of the 2-aminoheptylgly is the most potent on HFF cells after 48 h incubation. UV−vis, fluorescence, and CD spectroscopies were used for two selected compounds based on their size and solubility, and dipole moment (propylgly and 2-aminoheptylgly) was used to investigate their binding mechanism to DNA and HSA.

Because of the lower K_{app} values than typical intercalators, the interaction of both compounds with DNA and HSA can be assumed as H-binding and hydrophobic via groove binding. Nevertheless, electrostatic interaction cannot be ruled out. The K_{app} value obtained for DNA interaction with 2-amino-heptylgly (1.33 mM^{-1}) is more than propylgly (1.11 mM^{-1}), while the K_{app} value for the HSA-propylgly system (1.40 mM^{-1}) is more than HSA-2-aminoheptylgly formation (1.06 mM^{-1}). Also, in the fluorescence study, low values of K_b (0.15 and 0.23 M^{-1}) and n (1.87 and 1.15) for the propylgly and 2-aminoheptylgly, respectively, confirm that their mode of binding with DNA is groove binding. The viscosity study was done to prove the nature of DNA interaction with two candidate compounds. Related data noticed that groove binding is more probable. Finally, molecular docking studies were performed to explore the preferred mode of DNA and HSA interaction with compounds. According to these studies, octylgly (−5.55 kcal/mol) and *tert*-pentylgly (−4.5 kcal/mol), with the most negative value of docking energy, were more reactive than others for DNA and HSA, respectively. The results indicated that the presence of bulky aliphatic groups increased nonclassical hydrogen bonding such as C−H···O and hydrophobic interaction with DNA binding; thus, the activity may change. So, molecular docking simulation data confirm the experimental spectral DNA- or HSA-compound interactions.

■ ASSOCIATED CONTENT

Data Availability Statement

The datasets analyzed during the current study are available from the corresponding author upon reasonable request.

Ⓢ Supporting Information

The Supporting Information is available free of charge at https://pubs.acs.org/doi/10.1021/acsomega.3c02828.

Mass spectra (Figures S1−S9); ^{1}H NMR and ^{13}C NMR spectra (Figures S10−S20); experimental and computational IR spectra (Figure S21); BOILED-Egg model (Figure S22); alterations of absorbance of DNA/HSA (Figure S23); DNA/HSA binding position in docking study (Figures S24 and S25); ^{1}H and ^{13}C NMR spectral data (Tables S1−S11); experimental IR data (Table S12); ADME properties factors (Table S13); toxicity prediction (Table S14); docking results of DNA/HSA-ligand binding (Tables S15 and S16); binding energy DNA/HSA (Tables S17 and S18); and interaction data for AA-DNA/HSA (Tables S19 and S20) (PDF)

■ AUTHOR INFORMATION

Corresponding Author

Mahboube Eslami Moghadam − *Chemistry and Chemical Engineering Research Center of Iran, Tehran, Iran;* ⓞ orcid.org/0000-0002-4801-7018; Email: eslami_moghadam@ccerci.ac.ir, eslami_moghadam@yahoo.com

Authors

Ameneh Jafari − *Chemistry and Chemical Engineering Research Center of Iran, Tehran, Iran*

Hassan Mansouri-Torshizi − *Department of Chemistry, University of Sistan and Baluchestan, Zahedan, Iran*

Complete contact information is available at:
https://pubs.acs.org/10.1021/acsomega.3c02828

Author Contributions

M.E.M. designed and directed the project, synthesized metallodrugs and analyzed the data, checked results, and edited the draft. A.J. performed the experiments and wrote the article draft. H.M.-T. checked the results and revised and edited the draft.

Notes

The authors declare no competing financial interest.

■ ABBREVIATIONS

AA, amino acid; ADME, absorption, distribution, metabolism, and excretion; BBB, blood−brain barrier; CD, circular dichroism; DFT, density functional theory; DMSO, dimethyl sulfoxide; GI Abs, gastric absorption intake; Gly, glycine; HFF, human foreskin fibroblasts; IC$_{50}$, fifty percent of inhibitory concentration; LD50, median lethal dose; MEP, molecular electrostatic potential; MTT, (3-(4,5-dimethylthiazol-2-yl)-2,5-diphenyltetrazolium bromide; OECD, The Organization for Economic Co-operation and Development; PDB, Protein Data Bank; QCDs, quantum chemical descriptors; RT, room temperature; SMILE, simplified molecular-input line-entry system; propylamine, propan-1-amine; butylamine, butan-1-amine; *tert*-butylamine, 2-methylpropan-2-amine; *sec*-butyl-amine, butan-2-amine; pentylamine, pentan-1-amine; isopen-tylamine, 3-methylbutan-1-amine; *tert*-pentylamine, 2-methyl-

butan-2-amine; hexylamine, hexan-1-amine; 2-aminoheptyl-amine, (2R)-heptan-2-amine; octylamine, octan-1-amine

■ REFERENCES

(1) Wu, G.; Wu, Z.; Dai, Z.; Yang, Y.; Wang, W.; Liu, C.; Wang, B.; Wang, J.; Yin, Y. Dietary requirements of "nutritionally non-essential amino acids" by animals and humans. *Amino Acids* **2013**, *44*, 1107−1113.

(2) Ohsawa, S.; Tokushima, T.; Okada, K. Hydration of the zwitterionic and protonated forms of glycine betaine probed by soft X-ray emission spectroscopy coupled with chemometrics. *J. Phys. Chem. B* **2021**, *125*, 1881−1887.

(3) Wu, S.; Ye, Q.; Wu, D.; Tao, Y.; Kong, Y. Enantioselective recognition of chiral tryptophan with achiral glycine through the strategy of chirality transfer. *Anal. Chem.* **2020**, *92*, 11927−11934.

(4) Razak, M. A.; Begum, P. S.; Viswanath, B.; Rajagopal, S. Multifarious beneficial effect of nonessential amino acid, glycine: a review. *Oxid. Med. Cel. Longevityl* **2022**, *2022*, 1716701.

(5) Wang, M.; Zhao, Y.; Zhang, L.; Deng, J.; Qi, K.; Zhou, P.; Ma, X.; Wang, D.; Li, Z.; Wang, J.; Yang, J.; Lu, J. R.; Zhang, J.; Xu, H. Unexpected role of achiral glycine in determining the suprastructural handedness of peptide nanofibrils. *ACS Nano* **2021**, *15*, 10328−10341.

(6) Yan-Do, R.; Duong, E.; Manning Fox, J. E.; Dai, X.; Suzuki, K.; Khan, S.; Bautista, A.; Ferdaoussi, M.; Lyon, J.; Wu, X.; Cheley, S.; MacDonald, P. E.; Braun, M. A glycine-insulin autocrine feedback loop enhances insulin secretion from human β-cells and is impaired in type 2 diabetes. *Diabetes* **2016**, *65*, 2311−2321.

(7) Amelio, I.; Cutruzzolá, F.; Antonov, A.; Agostini, M.; Melino, G. Serine and glycine metabolism in cancer. *Trends Biochem. Sci.* **2014**, *39*, 191−198.

(8) Palantöken, S.; Bethke, K.; Zivanovic, V.; Kalinka, G.; Kneipp, J.; Rademann, K. Cellulose hydrogels physically crosslinked by glycine: Synthesis, characterization, thermal and mechanical properties. *J. Appl. Polym. Sci.* **2020**, *137*, 48380.

(9) Sánchez-Lara, E.; García-García, A.; González-Vergara, E.; Cepeda, J.; Rodríguez-Diéguez, A. Magneto-structural correlations of cyclo-tetravanadates functionalized with mixed-ligand copper (II) complexes. *New J. Chem.* **2021**, *45*, 5081−5092.

(10) Appleton, T. G.; Hall, J. R. Platinum (II) complexes with glycine as an oxygen-bound unidentate ligand. *J. Chem. Soc., Chem. Commun.* **1983**, *16*, 911−913.

(11) Abu-Dief, A. M.; Nassr, L. A. E. Tailoring, physicochemical characterization, antibacterial and DNA binding mode studies of Cu(II) Schiff bases amino acid bioactive agents incorporating 5-bromo-2-hydroxybenzaldehyde. *J. Iran. Chem. Soc.* **2015**, *12*, 943−955.

(12) Moghadam, M. E.; Sadeghi, M.; Mansouri-Torshizi, H.; Saidifar, M. High cancer selectivity and improving drug release from mesoporous silica nanoparticles in the presence of human serum albumin in cisplatin, carboplatin, oxaliplatin, and oxalipalladium treatment. *Eur. J. Pharm. Sci.* **2023**, *187*, No. 106477.

(13) Amir, M. K.; Khan, S. Z.; Hayat, F.; Hassan, A.; Butler, I. S.; Rehman, Z.-U. Anticancer activity, DNA-binding and DNA-denaturing aptitude of palladium(II) dithiocarbamates. *Inorg. Chim. Acta* **2016**, *451*, 31−40.

(14) Hafshajani, K. T.; Sohrabi, N.; Moghadam, M. E.; Oftadeh, M. Spectroscopy and molecular dynamic study of the interaction of calf thymus DNA by anticancer Pt complex with butyl glycine ligand. *Spectrochim. Acta, Part A* **2023**, *299*, No. 122826.

(15) Mohammadlou, F.; Mansouri-Torshizi, H.; Dehghanian, E.; Eslami-Moghadam, M.; Dusek, M.; Eigner, V. A new zinc (II) complex of 2-benzoimidazoledisulfide ligand: synthesis, X-ray crystallographic structure, investigation of CT-DNA and BSA interaction by spectroscopic techniques and molecular docking. *J. Photochem. Photobiol., A* **2023**, *443*, No. 114830.

(16) Safa Shams Abyaneh, F.; Eslami Moghadam, M.; Hossaini Sadr, M.; Divsalar, A. Effect of lipophilicity of amylamine and amylglycine

(17) Jaiswal, K. S.; Rathod, V. K. Green synthesis of amyl levulinate using lipase in the solvent free system: Optimization, mechanism and thermodynamics studies. *Catal. Today* **2021**, *375*, 120−131.

(18) Sheldon, R. A. The greening of solvents: Towards sustainable organic synthesis. *Curr. Opin. Green Sustainable Chem.* **2019**, *18*, 13−19.

(19) Lillian, E. D.; Bruce, A. D.; Ya-Dong, L.; David, D.; Alan, B. I. P; Brenda, K.; Kevin, R. Aliphatic amino carboxylic and amino phosphonic acids, amino nitriles, and amino tetrazoles as cellular rescue agents 2005, US 200/0159393 A1.

(20) Edward, S.; Martyn, P.; Mike, A. Pro-drug Compounds 2013, US 2014/0011773 A1.

(21) Tao, X.; Deng, Y.; Shen, Z.; Ling, J. Controlled polymerization of N-substituted glycine N-thiocarboxyanhydrides initiated by rare earth borohydrides toward hydrophilic and hydrophobic polypep-toids. *Macromolecules* **2014**, *47*, 6173−6180.

(22) Eslami Moghadam, M.; Saidifar, M.; Divsalar, A.; Mansouri-Torshizi, H.; Saboury, A. A.; Farhangian, H.; Ghadamgahi, M. Rich spectroscopic and molecular dynamic studies on the interaction of cytotoxic Pt (II) and Pd (II) complexes of glycine derivatives with calf thymus DNA. *J. Biomol. Struct. Dyn.* **2016**, *34*, 206−222.

(23) Ni, Y.; Sun, J.; Wei, Y.; Fu, X.; Zhu, C.; Li, Z. Two-dimensional supramolecular assemblies from pH-responsive poly (ethyl glycol)-b-poly (l-glutamic acid)-b-poly (N-octylglycine) triblock copolymer. *Biomacromolecules* **2017**, *18*, 3367−3374.

(24) Wu, Y.; Zhou, M.; Chen, K.; Chen, S.; Xiao, X.; Ji, Z.; Zou, J.; Liu, R. Alkali-metal hexamethyldisilazide initiated polymerization on alpha-amino acid N-substituted N-carboxyanhydrides for facile polypeptoid synthesis. *Chin. Chem. Lett.* **2021**, *32*, 1675−1678.

(25) Barata, K.; Yan, T.; Feringa, B. L. N-alkylated amino acids and oligopeptides, uses thereof and methods for providing them 2018, WO/2018/178397.

(26) *Gaussian 09, Revision D.01*, Frisch, M.J.; Trucks, G.W.; Schlegel, H.B.; Scuseria, G.E.; Robb, M.A.; Cheeseman, J.R.; Scalmani, G.; Barone, V.; Mennucci, B.; Petersson, G.A.; Nakatsuji, H. et al. Gaussian. Inc., Wallingford CT, 2009, *121*, 150−166.

(27) Dennington, R.; Keith, T.A.; Millam, J.M. *GaussView 6.0. 16*. Semichem Inc.: Shawnee Mission, KS, USA. 2016.

(28) Imran, M.; Zia-Ur-Rehman; Kondratyuk, T.; Bélanger-Gariepy, F. New ternary platinum(II) dithiocarbamates: synthesis, character-ization, anticancer, DNA binding and DNA denaturing studies. *Inorg. Chem. Commun.* **2019**, *103*, 12−20.

(29) Imran, M.; Rehman, Z. U.; Hogarth, G.; Tocher, D. A.; Chaudhry, G.-E.-S.; Butler, I. S.; Bélanger-Gariepy, F.; Kondratyuk, T. Two new monofunctional platinum(II) dithiocarbamate complexes: phenanthriplatin-type axial protection, equatorial-axial conformational isomerism, and anticancer and DNA binding studies. *Dalton Trans.* **2020**, *49*, 15385−15396.

(30) *ANNEX, PART A: METHODS FOR THE DETERMINATION OF PHYSICOCHEMICAL PROPERTIES*, COM-AC_DRC(**2007**) CMT-2007-2696-4_EN.

(31) Jagadeesan, S.; Balasubramanian, V.; Baumann, P.; Neuburger, M.; Häussinger, D.; Palivan, C. G. Water-soluble Co (III) complexes of substituted phenanthrolines with cell selective anticancer activity. *Inorg. Chem.* **2013**, *52*, 12535−12544.

(32) Daina, A.; Michielin, O.; Zoete, V. SwissADME: A free web tool to evaluate pharmacokinetics, drug-likeness and medicinal chemistry friendliness of small molecules. *Sci. Rep.* **2017**, *7*, 42717.

(33) Banerjee, P.; Eckert, A. O.; Schrey, A. K.; Preissner, R. ProTox-II: a webserver for the prediction of toxicity of chemicals. *Nucleic Acids Res.* **2018**, *46*, W257−W263.

(34) Al-Noor, T. H.; Mohapatra, R. K.; Azam, M.; Karem, L. K. A.; Mohapatra, P. K.; Ibrahim, A. A.; Parhi, P. K.; Dash, G. C.; El-ajaily, M. M.; Al-Resayes, S. I.; Raval, M. K.; Pintilie, L. Mixed-ligand complexes of ampicillin derived Schiff base ligand and Nicotinamide: Synthesis, physico-chemical studies, DFT calculation, antibacterial

study, and molecular docking analysis. *J. Mol. Struct.* **2021**, *1229*, No. 129832.

(35) Ramezani, N.; Eslami Moghadam, M.; Behzad, M. Investigating the anticancer properties of the two new platinum complexes with iso- and tert-pentylglycine by the DFT, molecular docking, and ADMET assessment and experimental confirmations. *JBIC J. Biol. Inorg. Chem.* **2021**, *26*, 283−298.

(36) Sharfalddin, A. A.; Emwas, A. H.; Jaremko, M.; Hussien, M. A. Synthesis and theoretical calculations of metal-antibiotic chelation with thiamphenicol: in vitro DNA and HSA binding, molecular docking, and cytotoxicity studies. *New J. Chem.* **2021**, *45*, 9598−9613.

(37) Feizi-Dehnayebi, M.; Dehghanian, E.; Mansouri-Torshizi, H. A novel palladium (II) antitumor agent: Synthesis, characterization, DFT perspective, CT-DNA, and BSA interaction studies via in-vitro and in-silico approaches. *Spectrochim. Acta, Part A* **2021**, *249*, No. 119215.

(38) Yinhua, D.; Foroughi, M. M.; Aramesh-Boroujeni, Z.; Jahani, S.; Peydayesh, M.; Borhani, F.; Khatami, M.; Rohani, M.; Dusek, M.; Eigner, V. The synthesis, characterization, DNA/BSA/HSA inter-actions, molecular modeling, antibacterial properties, and in vitro cytotoxic activities of novel parent and niosome nano-encapsulated Ho (III) complexes. *RSC Adv.* **2020**, *10*, 22891−22908.

(39) Revathi, N.; Sankarganesh, M.; Raja, J. D.; Vinoth Kumar, G. G.; Sakthivel, A.; Rajasekaran, R. Bio-active mixed ligand Cu(II) and Zn(II) complexes of pyrimidine derivative Schiff base: DFT calculation, antimicrobial, antioxidant, DNA binding, anticancer and molecular docking studies. *J. Biomol. Struct. Dyn.* **2021**, *39*, 3012−3024.

(40) Xiong, Y.; Gao, X.; Pan, D.; Zhang, T.; Qi, L.; Wang, N.; Zhao, Y.; Dang, Y. A strategy for screening novel umami dipeptides based on common feature pharmacophore and molecular docking. *Biomaterials* **2022**, *288*, No. 121697.

(41) Morris, G. M.; Huey, R.; Lindstrom, W.; Sanner, M. F.; Belew, R. K.; Goodsell, D. S.; Olson, A. J. AutoDock4 and AutoDockTools4: Automated docking with selective receptor flexibility. *J. Comput. Chem.* **2009**, *30*, 2785−2791.

(42) Nakamoto, K. Part B: applications in coordination, organo-metallic, and bioinorganic chemistry *Infrared and Raman spectra of inorganic and coordination compounds*, John Wiley & Sons, 2008.

(43) Rosado, M. T.; Duarte, M. L. T. S.; Fausto, R. Vibrational spectra of acid and alkaline glycine salts. *Vib. Spectrosc.* **1998**, *16*, 35−54.

(44) Folliet, N.; Gervais, C.; Costa, D.; Laurent, G.; Babonneau, F.; Stievano, L.; Lambert, J. F.; Tielens, F. A molecular picture of the adsorption of glycine in mesoporous silica through NMR experiments combined with DFT-D calculations. *J. Phys. Chem. C* **2013**, *117*, 4104−4114.

(45) Shimizu, A.; Ishizaki, Y.; Horiuchi, S.; Hirose, T.; Matsuda, K.; Sato, H.; Yoshida, J. I. HOMO−LUMO energy-gap tuning of π-conjugated zwitterions composed of electron-donating anion and electron-accepting cation. *J. Org. Chem.* **2021**, *86*, 770−781.

(46) Siddique, S. A.; Arshad, M.; Naveed, S.; Mehboob, M. Y.; Adnan, M.; Hussain, R.; Ali, B.; Siddique, M. B. A.; Liu, X. Efficient tuning of zinc phthalocyanine-based dyes for dye-sensitized solar cells: a detailed DFT study. *RSC Adv.* **2021**, *11*, 27570−27582.

(47) Muz, İ.; Kurban, M. Zinc oxide nanoclusters and their potential application as CH_4 and CO_2 gas sensors: Insight from DFT and TD-DFT. *J. Comput. Chem.* **2022**, *43*, 1839−1847.

(48) Hosseini-Hashemi, Z.; Eslami Moghadam, M.; Mirzaei, M.; Notash, B. Biological Activity of Two Anticancer Pt Complexes with a Cyclohexylglycine Ligand against a Colon Cancer Cell Line: Theoretical and Experimental Study. *ACS Omega* **2022**, *7*, 39794−39811.

(49) Wu, Y. R.; Tang, J. Q.; Zhang, W. N.; Zhuang, C. L.; Shi, Y. Rational drug design of CB2 receptor ligands: from 2012 to 2021. *RSC Adv.* **2022**, *12*, 35242−35259.

(50) Lipinski, C. A.; Lombardo, F.; Dominy, B. W.; Feeney, P. J. Experimental and computational approaches to estimate solubility and permeability in drug discovery and development settings. *Adv. Drug Delivery Rev.* **2012**, *64*, 4−17.

(51) Alaysuy, O.; Abumelha, H. M.; Alsoliemy, A.; Alharbi, A.; Alatawi, N. M.; Osman, H. E. M.; Zaky, R.; El-Metwaly, N. M. Elucidating of new hydrazide-based complexes derived from Pd(II), Cu(II), and Cd(II) ions: studies concerning spectral, DFT, Hirshfeld-crystal, biological screening beside Swiss-ADME verification. *J. Mol. Struct.* **2022**, *1259*, No. 132748.

(52) Sait, K. H. W.; Mashraqi, M.; Khogeer, A. A.; Alzahrani, O.; Anfinan, N. M.; Sait, H. K.; Almutairi, A.; Alam, Q. Molecular docking analysis of HER-2 inhibitor from the ZINC database as anticancer agents. *Bioinformation* **2020**, *16*, 882.

(53) Zargar Shooshtari, F.; Souri, M. K.; Hasandokht, M. R.; Jari, S. K. Glycine mitigates fertilizer requirements of agricultural crops: case study with cucumber as a high fertilizer demanding crop. *Chem. Biol. Technol. Agric.* **2020**, *7*, 1−10.

(54) Shiekhzadeh, A.; Sohrabi, N.; Moghadam, M. E.; Oftadeh, M. Kinetic and thermodynamic investigation of human serum albumin interaction with anticancer glycine derivative of platinum complex by using spectroscopic methods and molecular docking. *Appl. Biochem. Biotechnol.* **2020**, *190*, 506−528.

(55) Bazsefidpar, P.; Eftekhar, E.; Jahromi, M. Z.; Nikpoor, A. R.; Moghadam, M. E.; Zolghadri, S. In-vitro cytotoxicity and in-vivo antitumor activity of two platinum complexes with 1, 3-dimethyl pentyl glycine ligand against breast cancer. *J. Inorg. Biochem.* **2023**, *241*, No. 112144.

(56) Arif, R.; Rana, M.; Yasmeen, S.; Amaduddin; Khan, M. S.; Abid, M.; Khan, M. S.; Rahisuddin. Facile Synthesis of Chalcone Derivatives as Antibacterial Agents: Synthesis, DNA Binding, Molecular Docking, DFT and Antioxidant Studies. *J. Mol. Struct.* **2020**, *1208*, 127905−127918.

(57) Feizi-Dehnayebi, M.; Dehghanian, E.; Mansouri-Torshizi, H. Synthesis and characterization of Pd (II) antitumor complex, DFT calculation, and DNA/BSA binding insight through the combined experimental and theoretical aspects. *J. Mol. Struct.* **2021**, *1240*, No. 130535.

(58) Amir, M. K.; Khan, Z.; Ahmad, I.; Nasir, J. A.; Abbas, S.; Rehman, Z.; Din, F. U.; Kondratyuk, T.; Bélanger-Gariepy, F. New [Pt (S_2CNR_2) Cl (PAr_3)] complexes as anticancer agents. *Inorg. Chem. Commun.* **2022**, *136*, No. 109142.

(59) Kou, M.; Qin, F.; Lv, W.; Zhang, X.; Wang, Y.; Zhao, H.; Zhang, Z. Oxygen-varying correlated fluorescence for determining the Stern−Volmer constant of porphyrin. *J. Phys. Chem. Lett.* **2022**, *13*, 2007−2011.

(60) Parsekar, S. U.; Paliwal, K.; Haldar, P.; Antharjanam, P. K. S.; Kumar, M. Synthesis, characterization, crystal structure, DNA and HSA Interactions, and anticancer activity of a mononuclear Cu(II) complex with a Schiff base ligand containing a thiadiazoline moiety. *ACS Omega* **2022**, *7*, 2881−2896.

(61) Moghadam, M. E.; Rezaeisadat, M.; Mansouri-Torshizi, H.; Hosseinzadeh, S.; Daneshyar, H. New anticancer potential Pt complex with tertamyl dithiocarbamate ligand: Synthesis, DNA targeting behavior, molecular dynamic, and biological activity. *J. Mol. Liq.* **2023**, *379*, No. 121651.

(62) Maiti, S. K.; Kalita, M.; Singh, A.; Deka, J.; Barman, P. Investigation of DNA binding and bioactivities of thioether containing Schiff base Copper (II), Cobalt (II) and Palladium (II) complexes: Synthesis, characterization, spectrochemical study, viscosity measure-ment. *Polyhedron* **2020**, *184*, No. 114559.

(63) Feizi-Dehnayebi, M.; Dehghanian, E.; Mansouri-Torshizi, H. DNA/BSA binding affinity studies of new Pd (II) complex with SS and NN donor mixed ligands via experimental insight and molecular simulation: Preliminary antitumor activity, lipophilicity, and DFT perspective. *J. Mol. Liq.* **2021**, *344*, No. 117853.

(64) Khan, G. S.; Shah, A.; Rehman, Z.; Barker, D. Chemistry of DNA minor groove binding agents. *J. Photochem. Photobiol. B: Biol.* **2012**, *115*, 105−118.

(65) Hafshejani, K. T.; Sohrabi, N.; Moghadam, M. E.; Oftadeh, M. Investigation of the physico-chemical interaction of ct-DNA with

Anticancer Glycine Derivative of Pt-complex by applying docking and MD simulation methods and multi-spectroscopic techniques. *J. Mol. Struct.* **2022**, *1263*, No. 133115.

(66) Hosseini-Hashemi, Z.; Mirzaei, M.; Eslami Moghadam, M. Property evaluation of two anticancer candidate platinum complexes with N-isobutyl glycine ligand against human colon cancer. *BioMetals* **2022**, *35*, 987−1009.